CANCER

Tumor cell–intrinsic PD-1 promotes Merkel cell carcinoma growth by activating downstream mTOR-mitochondrial ROS signaling

Christina Martins[1,2], Erik Rasbach[1,2,3], Markus V. Heppt[1,4], Praveen Singh[1,2], Zsofi Kulcsar[1,2,5], Julia Holzgruber[1,2,6], Asmi Chakraborty[1,2], Kyla Mucciarone[7], Sonja Kleffel[1], Anne Brandenburg[1,5], Wolfram Hoetzenecker[6], Nuh N. Rahbari[3], James A. DeCaprio[8,9,10], Manisha Thakuria[1,10], George F. Murphy[7], Matthew R. Ramsey[1], Christian Posch[1,11,12,13], Steven R. Barthel[1,2], Tobias Schatton[1,2,14]*

Merkel cell carcinoma (MCC) is a rare and aggressive skin cancer. Inhibitors targeting the programmed cell death 1 (PD-1) immune checkpoint have improved MCC patient outcomes by boosting antitumor T cell immunity. Here, we identify PD-1 as a growth-promoting receptor intrinsic to MCC cells. In human MCC lines and clinical tumors, RT-PCR–based sequencing, immunoblotting, flow cytometry, and immunofluorescence analyses demonstrated PD-1 gene and protein expression by MCC cells. MCC–PD-1 ligation enhanced, and its inhibition or silencing suppressed, in vitro proliferation and in vivo tumor xenograft growth. Consistently, MCC–PD-1 binding to PD-L1 or PD-L2 induced, while antibody-mediated PD-1 blockade inhibited, protumorigenic mTOR signaling, mitochondrial (mt) respiration, and ROS generation. Last, pharmacologic inhibition of mTOR or mtROS reversed MCC–PD-1:PD-L1–dependent proliferation and synergized with PD-1 checkpoint blockade in suppressing tumorigenesis. Our results identify an MCC–PD-1–mTOR–mtROS axis as a tumor growth–accelerating mechanism, the blockade of which might contribute to clinical response in patients with MCC.

INTRODUCTION

The programmed cell death 1 (PD-1) pathway is a premier cancer drug target for immune checkpoint inhibitor (ICI) therapy (*1*). PD-1 engagement by its ligands, PD-L1 or PD-L2, dampens T effector functions by suppressing pro-proliferative signaling pathways downstream of the T cell receptor (*2*, *3*). This T cell regulatory process maintains immune homeostasis in healthy tissues by dampening aberrant T cell activation and consequent inflammation and autoimmunity. Cancers exploit the PD-1 pathway to evade tumor-directed T cell immunity to facilitate neoplastic progression (*4*). Accordingly, PD-1 axis blockade boosts antitumor T cell responses, thereby inhibiting tumor outgrowth in preclinical cancer models (*5*, *6*). In the clinic, therapeutic PD-1 and PD-L1 antibodies (Abs) have shown remarkable survival benefit for patients with advanced stage cancers of various etiology (*1*). Consequently, the United States Food and Drug Administration (FDA) has approved six PD-1 and three PD-L1 blocking Ab clones for the treatment of metastatic disease of diverse origin (*7*). Nonetheless, clinical benefit varies by individual patient and tumor entity (*8*).

Merkel cell carcinoma (MCC) is a highly aggressive neuroendocrine carcinoma of the skin that responds exceptionally well to PD-1–targeted ICI therapy (*9*, *10*). Although relatively rare, MCC incidence and mortality have been rapidly increasing in recent decades (*11*). Risk of MCC development increases with advanced age (*9*), which also correlates with improved ICI outcomes (*12*). MCC occurrence is further linked to genetic mutations induced by ultraviolet radiation and infection with Merkel cell polyomavirus (*9*, *13*). Both processes augment tumoral immunogenicity and consequent recognition by T cells (*7*), thus potentially contributing to robust PD-1 ICI benefit in patients with MCC.

Several additional facets of PD-1 immunobiology warrant consideration in interpreting and optimizing ICI efficacy. For example, tumor immune infiltrates other than T cells are also known to express PD-1, including B cells, macrophages, and natural killer cells (*14*–*16*). PD-1 inhibition on these cell types suppresses tumor growth and prolongs patient survival. PD-1 has also been found directly on cancer cells in several tumor entities (*17*–*26*). In preclinical tumor models, including melanoma, hepatocellular carcinoma, and glioblastoma, cancer cell–intrinsic PD-1 promotes tumorigenesis, and its blockade thwarts cancer growth, including in the absence of functional T cell immunity (*17*–*19*, *24*, *27*). Conversely, tumor PD-1 is growth-suppressive in non–small cell lung and colorectal carcinoma cells, such that its antagonism promotes disease progression (*21*–*23*, *25*, *26*). Whether PD-1 is expressed by MCC cells, is recognized by FDA-approved inhibitors, and stimulates or suppresses tumor growth is now unknown. More broadly, the precise signaling effectors mediating cancer cell–PD-1–dependent tumorigenesis and

[1]Department of Dermatology, Brigham and Women's Hospital, Harvard Medical School, Boston, MA 02115, USA. [2]Program of Glyco-Immunology and Oncology, Brigham and Women's Hospital, Harvard Medical School, Boston, MA 02115, USA. [3]Department of Surgery, University Hospital Mannheim, Heidelberg University, 68167 Mannheim, Germany. [4]Department of Dermatology, University Hospital Erlangen, Friedrich-Alexander-University (FAU), 91054 Erlangen, Germany. [5]Department of Dermatology, University Hospital Bonn, 53127 Bonn, Germany. [6]Department of Dermatology and Venerology, Johannes Kepler University, 4020 Linz, Austria. [7]Department of Pathology, Brigham and Women's Hospital, Harvard Medical School, Boston, MA 02115, USA. [8]Department of Medical Oncology, Dana-Farber Cancer Institute, Harvard Medical School, Boston, MA 02115, USA. [9]Program in Virology, Graduate School of Arts and Sciences, Harvard University, Cambridge, MA 02138, USA. [10]Merkel Cell Carcinoma Center of Excellence, Dana-Farber/Brigham and Women's Hospital Cancer Center, Boston, MA 02115, USA. [11]Department of Dermatology, Vienna Healthcare Group, 1130 Vienna, Austria. [12]Faculty of Medicine, Sigmund Freud University Vienna, 1020 Vienna, Austria. [13]Department of Dermatology and Allergy, School of Medicine, Technical University of Munich, 81675 Munich, Germany. [14]Department of Medicine, Boston Children's Hospital, Harvard Medical School, Boston, MA 02115, USA.
*Corresponding author. Email: tschatton@bwh.harvard.edu

if their targeting synergizes with PD-1 ICI–based growth inhibition have not been well defined for any cancer type.

Here, we report PD-1 gene and protein expression directly by MCC cells in several established human lines and patient tumor biospecimens. MCC-expressed PD-1 is recognized by independent Ab clones, including the FDA-approved PD-1 clinical inhibitor, nivolumab. MCC–PD-1 engagement by its ligands, PD-L1 or PD-L2, promotes in vitro tumor cell growth. Conversely, Ab-mediated MCC–PD-1 blockade or genetic knockdown (KD) suppresses in vitro proliferation and in vivo human tumor xenograft growth in immunocompromised nonobese diabetic (NOD)–severe combined immunodeficient (SCID) IL-2 receptor γ (IL-2Rγ) chain–null (NSG) mice. Consistently, PD-1 receptor ligation induces, while its blockade by nivolumab inhibits, phosphorylation of the protumorigenic mammalian target of rapamycin (mTOR) pathway effectors, mTOR and proline-rich AKT substrate 40 kDa (PRAS40), as well as downstream mitochondrial (mt) respiration and reactive oxygen species (ROS) generation. Pharmacologic inhibition of mTOR with rapamycin or of mtROS using the antioxidants, *N*-acetylcysteine (NAC), or mito–2,2,6,6-tetramethylpiperidinyloxyl (TEMPO) (*28*–*31*) reverses MCC–PD-1–mediated tumor cell growth. Together, these data establish expression of PD-1 by MCC cells and its recognition and functional inhibition by an FDA-approved PD-1 blocking agent, nivolumab. Furthermore, our findings reveal a protumorigenic, cancer cell–intrinsic PD-1:PD-L1 signaling circuit, mTOR-PRAS40-mtROS, the inhibition of which suppresses MCC–PD-1–dependent tumorigenesis and synergizes with PD-1 checkpoint blockade in thwarting tumor growth.

RESULTS

MCCs contain PD-1–expressing tumor cells

Immunofluorescence (IF) triple labeling of clinical MCC biospecimens for PD-1 with the MCC marker (*32*), cytokeratin 20 (CK20), and the leukocyte common antigen, CD45, revealed PD-1 protein expression by $CK20^+CD45^-$ tumor cells in 11 of the 13 patients with MCC (Fig. 1A). Flow cytometric analysis of tumor-derived single cells from clinical MCC specimens additionally confirmed PD-1 expression by 16.3 ± 0.8% of MCC cells (means ± SD, $n = 3$), defined as $CD56^+CD45^-$ (*33*), and by 26.1 ± 0.8% of $CD45^+$ tumor-infiltrating lymphocytes (TILs) using the MIH4 anti-human PD-1 Ab clone (Fig. 1B). The FDA-approved clinical PD-1 blocking Ab, nivolumab (*7*), also bound PD-1 on 9.6 ± 1.2% of patient MCC cells and 23.4 ± 2.6% of respective TILs (Fig. 1B). $CD56^+CD45^-$ cell frequency exceeded 90% in the human MCC lines, MKL-1, MKL-2, MS-1, and WaGa, thereby confirming utility of this marker combination for MCC cell detection (fig. S1A). Reverse transcription quantitative polymerase chain reaction (RT-qPCR) demonstrated PD-1 gene (*PDCD1*) expression by all four MCC lines at levels significantly exceeding those in human A375 melanoma cells (Fig. 1C) previously shown to express PD-1 (*18*, *20*, *21*). In contrast, gene expression of PD-1 ligands, PD-L1 (*CD274* and *PDCD1LG1*) and PD-L2 (*PDCD1LG2*), was substantially lower in MCC versus A375 melanoma cells (fig. S1B). RT-PCR amplification and sequencing of the full *PDCD1* coding sequence further confirmed the PD-1 gene transcript in all four MCC lines (Fig. 1D). PD-1 protein expression by MKL-1, MKL-2, MS-1, and WaGa cells was detected by immunoblot analysis at the molecular weight corresponding to positive control T cell–PD-1 (Fig. 1E) and by fluorescence-activated cell sorting (FACS) analysis at mean $PD\text{-}1^+$ cell frequencies ranging from 21.2 ± 2.9% to 42.6 ± 4.1% (± SEM; Fig. 1F). Consistent with the RT-qPCR results above (Fig. 1C and fig. S1B), mean PD-L1 and PD-L2 surface protein levels were low (<2% positivity) across all MCC lines (fig S1C). Notably, PD-1 gene expression was markedly enhanced in MCC tumor xenografts compared to that in respective in vitro cultures (Fig. 1G). $PD\text{-}1^+$ MCC cell frequencies in vivo fell within the already substantial ranges observed in vitro (Fig. 1F and fig. S1D). Nonetheless, the levels of tumor cell–PD-1 [mean fluorescence intensity (MFI)] were significantly increased even further on WaGa tumor xenografts compared to that on respective cell line cultures (fig S1D), suggestive of MCC-intrinsic PD-1 receptor activity in tumorigenesis.

MCC–PD-1 ligation promotes and its blockade inhibits tumor growth

To dissect MCC–PD-1 functions in tumorigenesis, we first examined whether its ligation modulates tumor cell growth. Addition of recombinant PD-L1 or PD-L2 immunoglobulin (Ig) to MKL-1, MKL-2, MS-1, or WaGa cultures significantly increased MCC cell proliferation by up to 3.2- or 2.3-fold, respectively, compared to control Ig treatment, as determined by CellTiter-Glo–based luminescence analysis (Fig. 2A). Neither PD-L1 nor PD-L2 significantly affected cell viability versus control Ig as determined by annexin V and propidium iodide (PI) flow cytometric staining (fig S2A), thus substantiating pro-proliferative as opposed to survival activity of MCC–PD-1. Incubation of MCC cultures with the PD-1 blocking Ab, nivolumab, significantly decreased in vitro tumor cell growth (Fig. 2B) but did not induce cell death relative to isotype-matched control Ab (fig. S2B). Anti-human PD-1 blocking Ab (J116 or nivolumab) administration to NSG mice lacking T cells and other adaptive immune cell subsets significantly inhibited MKL-1, MKL-2, MS-1, and WaGa tumor xenograft growth compared to respective isotype-matched control groups (Fig. 2C). Flow cytometric analysis validated specificity of both PD-1 Ab clones used above for human MCC and human positive T cell controls, but not murine T cells (<1% reactivity; fig. S2C), thus supporting an MCC–PD-1–directed effect. Consistently, short hairpin RNA (shRNA)-mediated KD of *PDCD1* directly in MKL-1 and WaGa cells, as authenticated by RT-qPCR, immunoblotting, and flow cytometry (fig. S3, A to C), significantly inhibited in vitro proliferation (fig. S3D) and in vivo tumor xenograft growth compared to respective scrambled control MCC cells (fig. S3E). In agreement with the more pronounced growth inhibitory effect of PD-1 blockade on MKL-2 and WaGa versus MKL-1 and MS-1 xenografts, combined PD-1 and PD-L1 in vivo gene expression levels were highest in the former two compared to that in the latter two tumor types (Fig. 1G and fig. S4A). MCC–PD-L1 protein levels (MFI) were also substantially elevated in vivo compared to that in respective in vitro lines (fig. S4B) and significantly enriched in $PD\text{-}1^+$ versus $PD\text{-}1^-$ tumor xenograft subsets (fig. S4C). Consistent with the negligible expression of PD-L1 on in vitro cultured MCC lines (fig. S1C), treatment of MKL-2 and WaGa cultures with anti-human PD-L1 blocking Ab did not significantly affect in vitro proliferation (fig. S4D). In contrast, administration of this anti-human PD-L1 Ab to NSG mice significantly suppressed MKL-2 and WaGa xenograft growth compared to isotype control Ab treatment (Fig. 2D), while anti-mouse PD-L1 blocking Ab had no significant effect (fig. S4E). Together, these results identify MCC-intrinsic PD-1 receptor:PD-L1 ligand interactions as

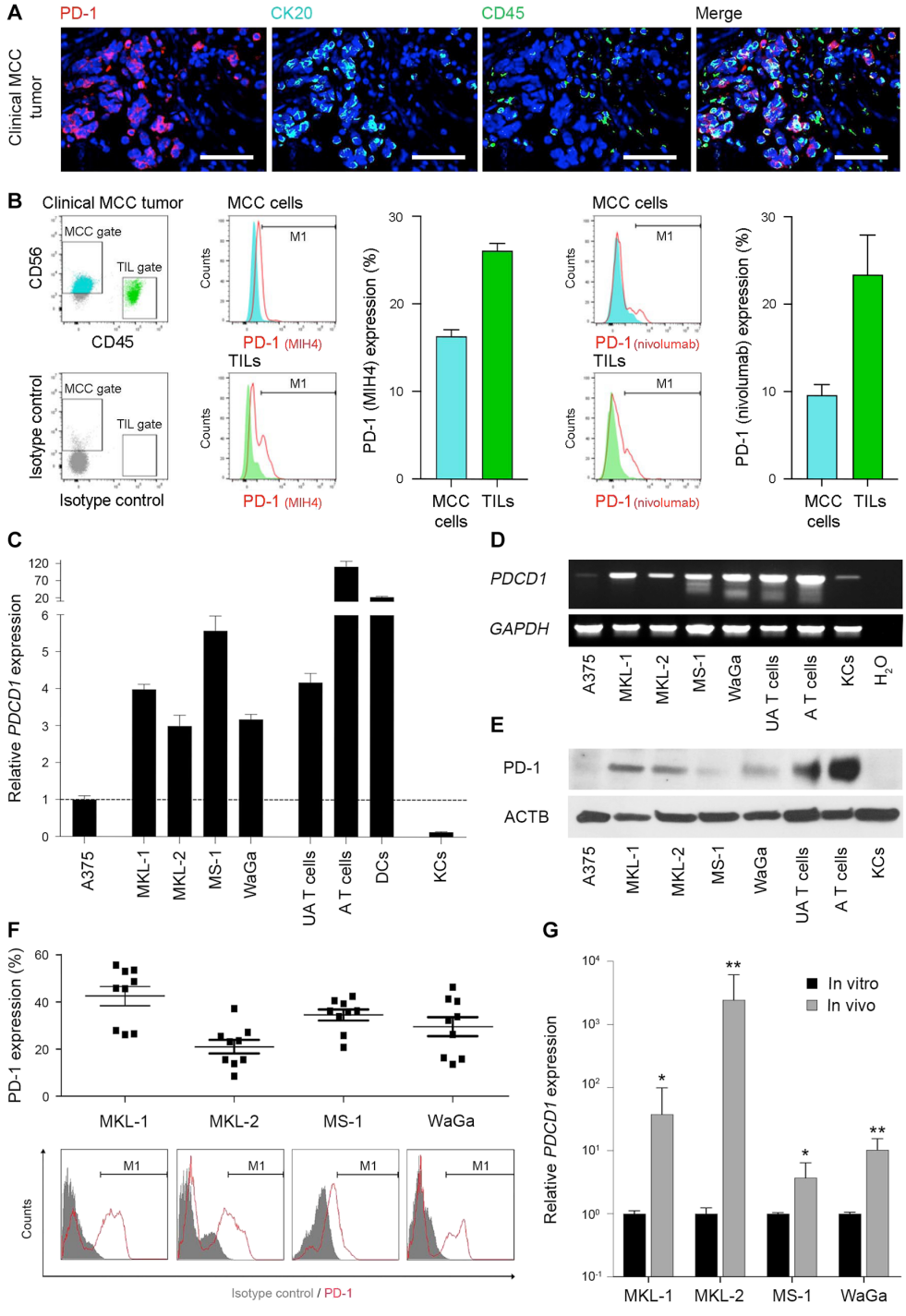

Fig. 1. PD-1 expression by MCC cells. (**A**) Representative triple immunofluorescence (IF) staining of a clinical MCC biopsy for PD-1 (red); the MCC marker, CK20 (aqua marine); and the pan-lymphocyte antigen, CD45 (green). Nuclei were counterstained with 4′,6-diamidino-2-phenylindole (DAPI) (blue). Size bars, 50 μm. (**B**) Representative flow cytometric analysis of PD-1 surface protein and mean expression (± SD) by MCC cells ($CD56^{+}CD45^{-}$) versus tumor-infiltrating lymphocytes (TILs; $CD45^{+}$) in a single-cell suspension derived from a clinical MCC tumor biospecimen, as determined by the PD-1 Ab clone MIH4 (left) and the FDA-approved inhibitor nivolumab (right). (**C**) Relative PDCD1 gene expression (means ± SEM) by human MCC lines, MKL-1, MKL-2, MS-1, and WaGa; unactivated (UA) and activated (A) human T cells; dendritic cells (DCs); and keratinocytes (KCs) versus human A375 melanoma cells, as determined by real-time quantitative reverse transcription polymerase chain reaction (RT-PCR). (**D**) RT-PCR expression analysis of the full-length PDCD1 coding sequence by MCC lines, as in (C), UA and A T cell positive controls; KCs; and A375 melanoma cells. Human glyceraldehyde-3-phosphate dehydrogenase (GAPDH) served as a housekeeping gene. (**E**) Immunoblot of PD-1 protein expression by cell types as in (D). Human actin beta (ACTB) served as a loading control. (**F**) Percentages (means ± SEM) and representative flow cytometric histograms of PD-1 surface protein expression by MCC cell lines. (**G**) Relative PDCD1 gene expression (fold change, means ± SEM) by MCC cells cultured in vitro versus respective MCC xenografts grown in NSG mice. Results are representative of $n = 13$ patients with MCC, at least $n = 5$ mice per experimental group and $n = 3$ independent experiments each. $^{*}P < 0.05$; $^{**}P < 0.01$. See also fig. S1.

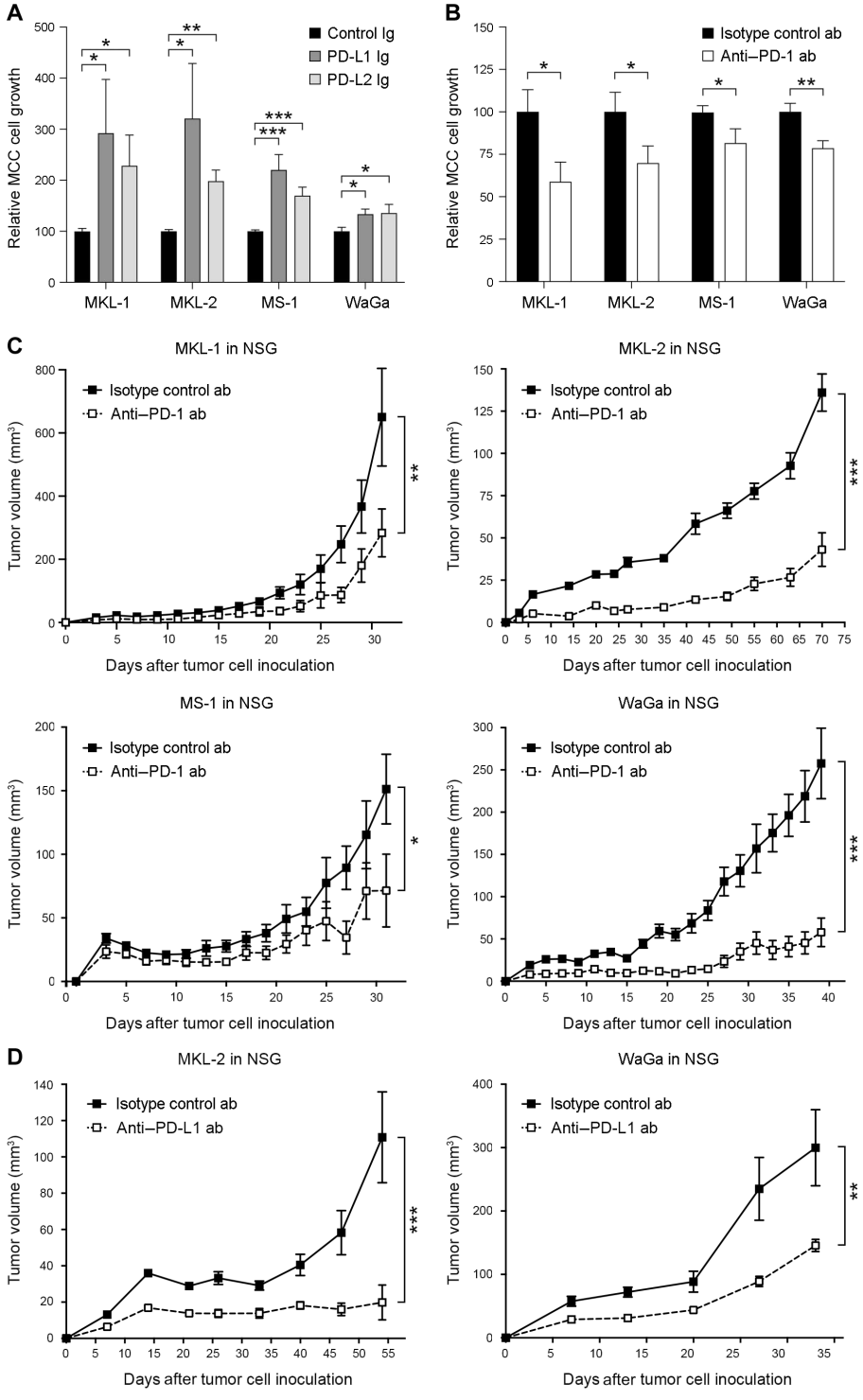

Fig. 2. MCC–PD-1 ligation promotes and its blockade inhibits tumor growth. Relative MCC tumor cell growth (means ± SEM) of MKL-1, MKL-2, MS-1, or WaGa cultures treated with (**A**) PD-L1 Ig or PD-L2 Ig versus control Ig or with (**B**) anti–PD-1 (nivolumab) versus isotype control Ab, as determined by CellTiter-Glo–based luminescence analysis. Results are representative of at least $n = 3$ independent experiments each. (**C**) Tumor growth kinetics (means ± SEM) of MKL-1, MKL-2, MS-1, or WaGa cells grafted to NSG mice treated with anti-human PD-1 blocking (J116 for MKL-1, MS-1, and WaGa; and nivolumab for MKL-2) versus isotype-matched control Ab ($n = 5$ to 19 mice per experimental group) or of (**D**) MKL-2 or WaGa cells in NSG mice treated with anti-human PD-L1 blocking versus isotype control Ab ($n = 6$ to 8 mice per group). *$P < 0.05$; **$P < 0.01$; ***$P < 0.001$. See also figs. S2 to S4.

growth-promoting mechanisms, the blockade of which suppresses tumorigenesis.

MCC–PD-1 activates downstream mTOR signaling, mitochondrial respiration, and ROS generation

Because various pro-proliferative signaling pathways, including mitogen-activated protein kinase (MAPK), phosphatidylinositol 3-kinase (PI3K)/AKT, and mTOR, have been identified as tumor cell–intrinsic PD-1 receptor targets in other malignancies (*17*, *18*, *23*, *26*, *27*, *34*, *35*), we next examined whether these pathways are also active in MCC cells. In contrast to A375 melanoma cells, phosphorylated (p-) extracellular signal–regulated kinase 1/2 (ERK1/2), AKT, or S6 were not detected in native MCC cell MKL-1, MKL-2, MS-1, or WaGa lysates by immunoblotting (Fig. 3A). Conspicuously, all four MCC lines expressed significant levels of the mTOR signaling effectors, p-mTOR, and p-PRAS40 (Fig. 3A). Compared to control Ig, recombinant PD-L1 or PD-L2 Ig treatment significantly induced phosphorylation of both mTOR and PRAS40 across all MCC lines (Fig. 3B). Conversely, addition of the PD-1 blocking Ab, nivolumab, to MCC cultures suppressed PD-L1– and PD-L2–mediated induction of p-mTOR and p-PRAS40 (Fig. 3C). The mTOR-PRAS40 signaling pathway is known to act in concert with mtROS to promote tumor growth (*36*, *37*). To thus examine whether MCC–PD-1 receptor activation triggers downstream mtROS production and mTOR signaling (Fig. 3), MCC lines were treated as above with PD-L1 or PD-L2 in the presence or absence of anti–PD-1 blocking Ab. PD-L1 and PD-L2 significantly induced, while PD-1 blockade antagonized, mtROS generation in MKL-2 and WaGa cells, as determined by MitoSOX Red–based FACS analysis (Fig. 4A). MCC–PD-1 ligation did not significantly compromise mitochondrial membrane integrity as assessed by MitoTracker Deep Red labeling (fig. S5A) or induce cytoplasmic ROS (determined by 2′,7′-dichlorodihydrofluorescein diacetate (H2DCFDA) staining; fig. S5B), of which both processes have been associated with cell death (*38*). Consistent with PD-L1– and PD-L2–mediated mtROS formation in MCC cells and their suppression by nivolumab blockade (Fig. 4A), PD-1 ligands significantly induced mitochondrial respiration [i.e., oxygen consumption rate (OCR)], while MCC–PD-1 blockade neutralized this pro-growth (*38*) effect (Fig. 4B). Glycolysis [measured as extracellular acidification rate (ECAR; fig. S5C] or uptake of the glucose analog, 2-(7-nitro-2,1,3-benzoxadiazol-4-yl)-D-glucosamine (2-NBDG) (fig. S5D) was not significantly affected by MCC–PD-1 receptor ligand engagement. To assess whether mTOR signaling is necessary for MCC–PD-1–mediated mtROS generation and mitochondrial respiration, MKL-2 and WaGa lines were stimulated with PD-L1 or PD-L2, as above, with or without the mTOR small-molecule inhibitor, rapamycin. Pharmacologic inhibition of mTOR significantly reversed PD-1 ligand–induced mtROS production (Fig. 4C) and OCR (Fig. 4D) in both MCC lines. Consistently, neutralization of downstream mtROS using two independent mitochondria-targeted antioxidant compounds (*28*–*31*), NAC (Fig. 5, A and B) and mito-TEMPO (Fig. 5, C and D), showed similar inhibition of PD-1 ligand–induced mtROS generation and OCR as antagonism of upstream mTOR in MKL-2 and WaGa cells. Together, these results identify an mTOR-mtROS circuit as a major downstream signaling target of the MCC-intrinsic PD-1 receptor.

Inhibition of mTOR or mitochondrial ROS reverses MCC–PD-1–dependent tumor growth

We next examined whether inhibition of the MCC-intrinsic mTOR-mtROS pathway blocks MCC–PD-1–dependent tumor cell growth, using FDA-approved or investigational agents. mtROS neutralization with the antioxidant scavenging agents (*28*–*31*), NAC (Fig. 6A) or mito-TEMPO (Fig. 6B), markedly suppressed MCC culture growth mediated by PD-L1 or PD-L2. Consistently, in vivo administration of either antioxidant compound significantly inhibited tumorigenesis of MKL-2 or WaGa tumor xenografts in NSG mice compared to that in vehicle control treatment (fig. S6A). In agreement with herein demonstrated MCC–PD-1–dependent induction of mtROS and mitochondrial respiration via mTOR (Fig. 4, C and D), inhibition of mTOR by rapamycin significantly counteracted PD-1 ligand–stimulated MKL-2 and WaGa proliferation (Fig. 6C). Combination therapy with nivolumab and rapamycin resulted in significantly reduced MKL-2 and WaGa tumor xenograft volumes in T cell–deficient NSG mice compared to those in either inhibitor alone (Fig. 6D). Therapeutic efficacy in this model was equally robust, independent of the order of treatment, that is whether nivolumab or rapamycin was administered first or second relative to the other (fig. S6B). Together, these findings identify the MCC-intrinsic PD-1–mTOR–mtROS axis as a tumor growth–accelerating mechanism, the therapeutic inhibition of which thwarts MCC tumorigenesis (Fig. 7).

DISCUSSION

PD-1 is an immune checkpoint receptor predominantly studied in T cells, owing to its ability to trigger T effector cell exhaustion and promote tumor immune evasion (*4*). PD-1 pathway blockade boosts T cell antitumor immunity and has yielded remarkable benefit for patients with metastatic disease of diverse origin (*7*). Accordingly, PD-1 has emerged as the premier target for ICI-based cancer therapy, as evidenced by the FDA approval of six distinct PD-1 blocking Abs: cemiplimab, dostarlimab, toripalimab, nivolumab, pembrolizumab, and retifanlimab (*1*), including the latter two for MCC (*10*). Using several independent methodologies, such as RT-PCR–based sequencing, immunoblotting, FACS, and IF analyses, our study now reveals functional PD-1 expression intrinsic to cancer cells in established human MCC cell lines and patient MCC biospecimens at levels approaching those in T cells. Notably, MCC–PD-1 was recognized not only by research-grade Abs but also by the clinically approved inhibitor, nivolumab, raising the possibility that cancer cell–PD-1 blockade might contribute to clinical benefit independent of and in addition to T cell–PD-1 inhibitory effects. Nivolumab-mediated PD-1 antagonism or *PDCD1* silencing significantly suppressed both in vitro proliferation and in vivo tumor xenograft growth of human MCC lines in NSG mice lacking T cell immunity, supporting such an MCC cell–directed effect of PD-1 checkpoint blockade.

Tumor cell–intrinsic PD-1 expression has also been reported in several additional malignancies, including melanoma (*17*–*21*, *39*, *40*), glioblastoma (*24*), hepatocellular (*27*), non–small cell lung (*21*, *22*, *25*), and colorectal carcinoma (*23*, *25*, *26*). Similar to our findings in MCC, cancer cell–expressed PD-1 promoted tumorigenesis in the first three cancers, while inhibiting growth in the latter two. MCC–PD-1 levels markedly exceeded those in melanoma, as directly demonstrated herein and when compared to published reports (*17*, *18*, *20*, *21*, *39*, *40*), consistent with the more pronounced growth inhibitory effect of PD-1 blockade in MCC- versus melanoma-bearing (*17*, *18*, *20*) NSG mice, particularly for MKL-2 and WaGa xenografts. These MCC tumors also expressed the highest levels of PD-L1 in comparison to MKL-1 and MS-1 xenografts, in

agreement with the demonstrated growth inhibitory effect of MCC–PD-L1 blockade in vivo but not in vitro and the established association of PD-L1 positivity with ICI response and survival in patients with MCC (*41*–*43*) and several other cancers (*1*). In contrast to malignancies like melanoma (*18*, *44*), PD-1 ligand expression by MCC cells was low to absent in vitro but substantially induced in vivo for some lines, highlighting unique PD-1:PD-L1 intracellular or intercellular interactions, expression patterns, regulation, and functions among distinct cell lines and cancer types.

The precise downstream signaling effector networks or mechanisms through which cancer cell–intrinsic PD-1 regulates tumorigenesis have not been previously defined in detail for any cancer

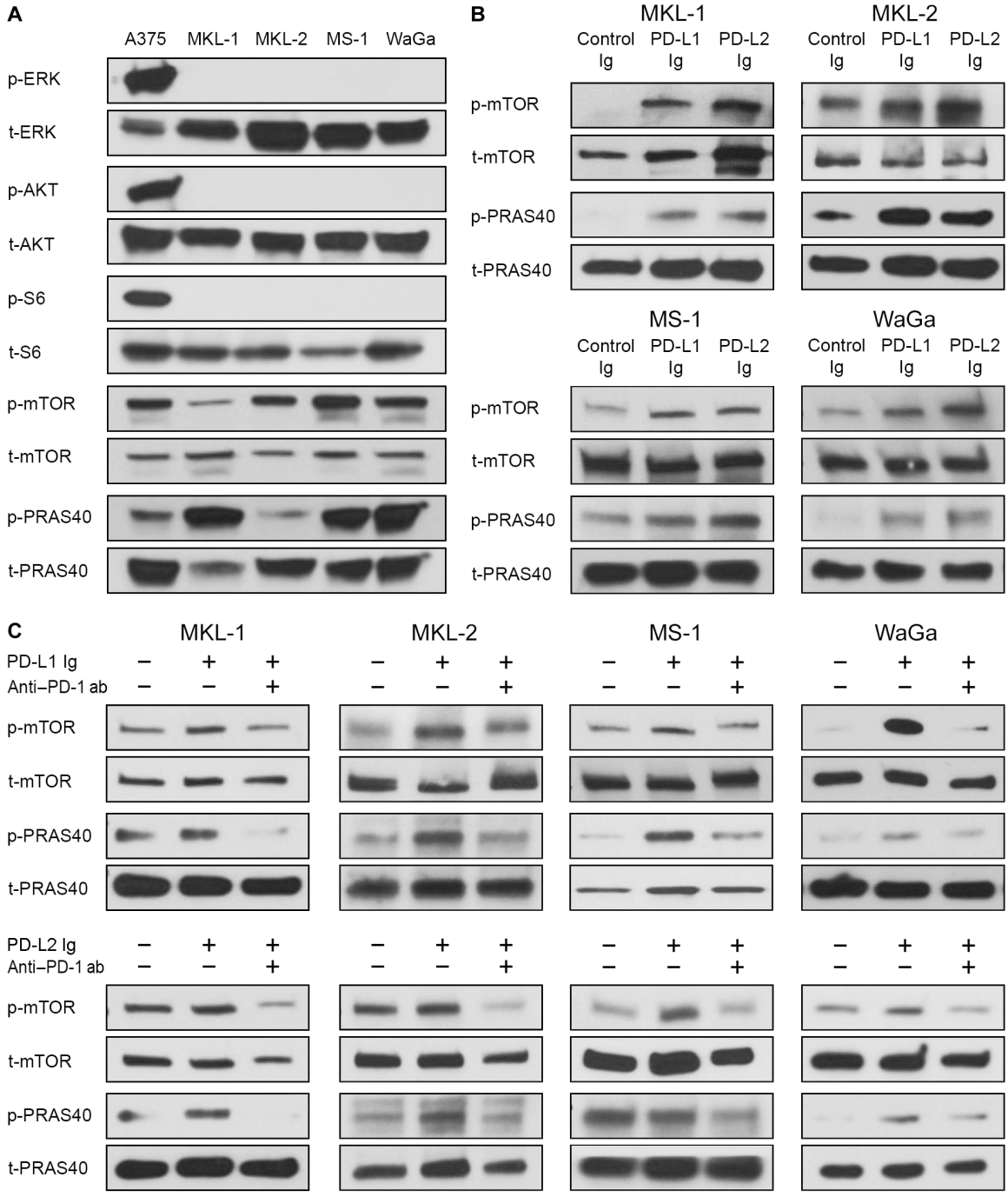

Fig. 3. The MCC–PD-1 receptor activates downstream mTOR signaling effectors. (**A**) Immunoblots of phosphorylated (p-) and total (t-) ERK, AKT, S6, mTOR, and PRAS40 in human MKL-1, MKL-2, MS-1, and WaGa MCC versus A375 melanoma cells. (**B**) Immunoblots of p- and t-mTOR and PRAS40 in MCC lines, as above, treated with PD-L1 or PD-L2 versus control Ig, (**C**) with or without anti–PD-1 (nivolumab) versus isotype control Ab. Results are representative of at least $n = 3$ independent experiments each.

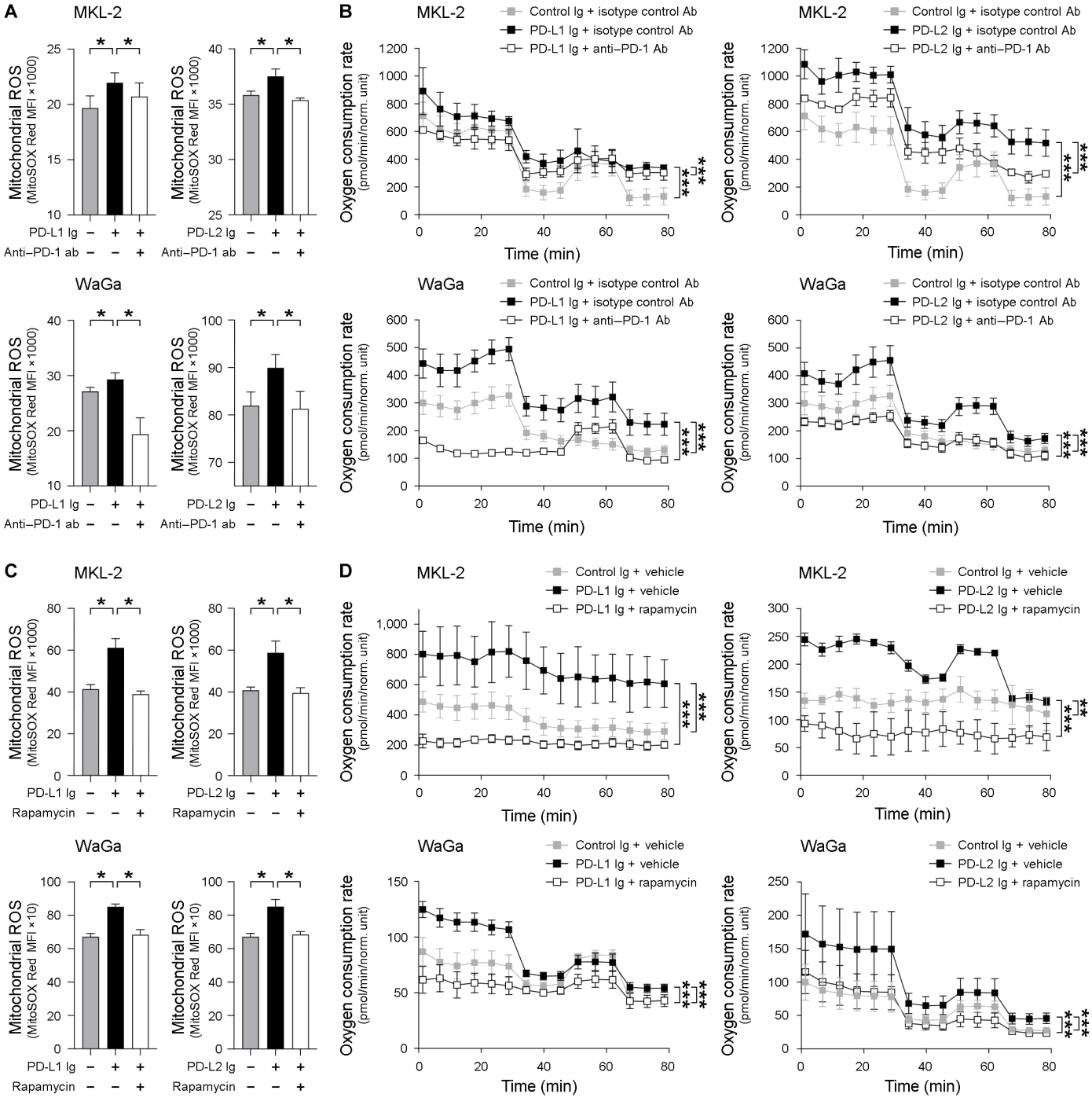

Fig. 4. MCC–PD-1 promotes mitochondrial ROS production and oxygen consumption. (**A**) Flow cytometric analysis of mtROS levels (MitoSOX Red MFI, means ± SEM) or (**B**) respiratory oxygen consumption rate (OCR; pmol/min per normalized unit) determined by Seahorse real-time cell metabolic analysis in MKL-2 (top) or WaGa (bottom) cultures treated with PD-L1 Ig (left) or PD-L2 Ig (right) versus control Ig, with or without anti–PD-1 blocking versus isotype control Ab. (**C**) Flow cytometric analysis of mtROS levels or (**D**) OCR, as determined above, in MKL-2 (top) or WaGa (bottom) cultures treated with PD-L1 Ig (left) or PD-L2 Ig (right) versus control Ig, in the presence or absence of the mTOR pharmacologic inhibitor, rapamycin versus vehicle control. Results are representative of at least $n = 3$ independent experiments each. The control Ig groups were acquired concurrently with PD-L1 Ig and PD-L2 Ig treatment and are thus identical for some cell lines. *$P < 0.05$; **$P < 0.01$; ***$P < 0.001$. See also fig. S5.

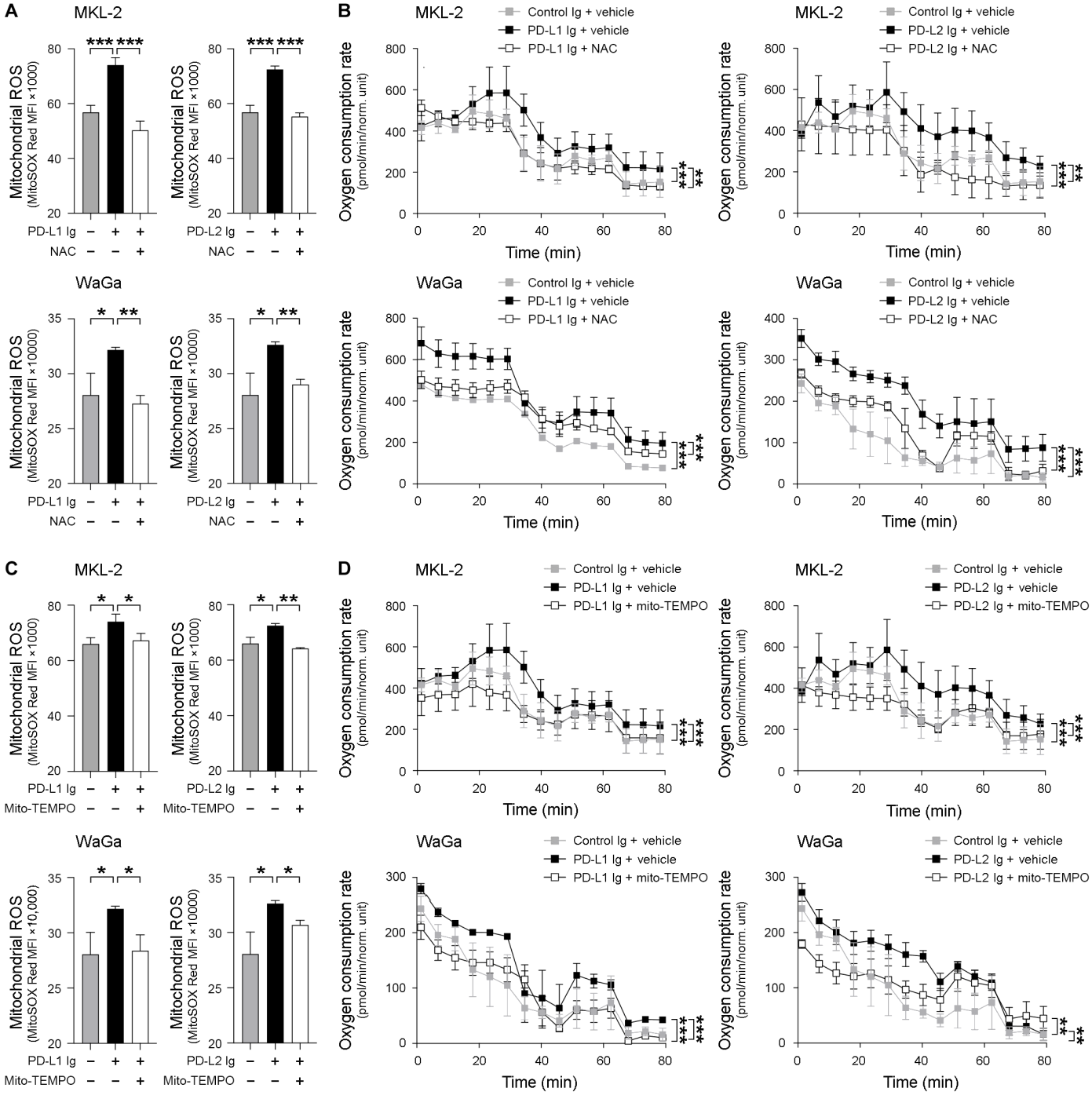

Fig. 5. Mitochondria-targeted antioxidants reverse MCC–PD-1–induced mtROS production and oxygen consumption. (**A**) Flow cytometric analysis of mtROS levels (MitoSOX Red MFI, means ± SEM) or (**B**) respiratory OCR (pmol/min per normalized unit) determined by Seahorse real-time cell metabolic analysis in MKL-2 (top) or WaGa (bottom) cultures treated with PD-L1 Ig (left) or PD-L2 Ig (right) versus control Ig, with or without NAC. (**C**) Flow cytometric analysis of mtROS levels or (**D**) OCR, as determined above, in MKL-2 (top) or WaGa (bottom) cultures treated with PD-L1 Ig (left) or PD-L2 Ig (right) versus control Ig, in the presence or absence of the mitochondria-targeted antioxidant, mito-TEMPO. Results are representative of at least $n = 3$ independent experiments each. The control Ig groups were acquired concurrently with PD-L1 Ig and PD-L2 Ig treatment and are thus identical for some cell lines. $^{*}P < 0.05$; $^{**}P < 0.01$; $^{***}P < 0.001$.

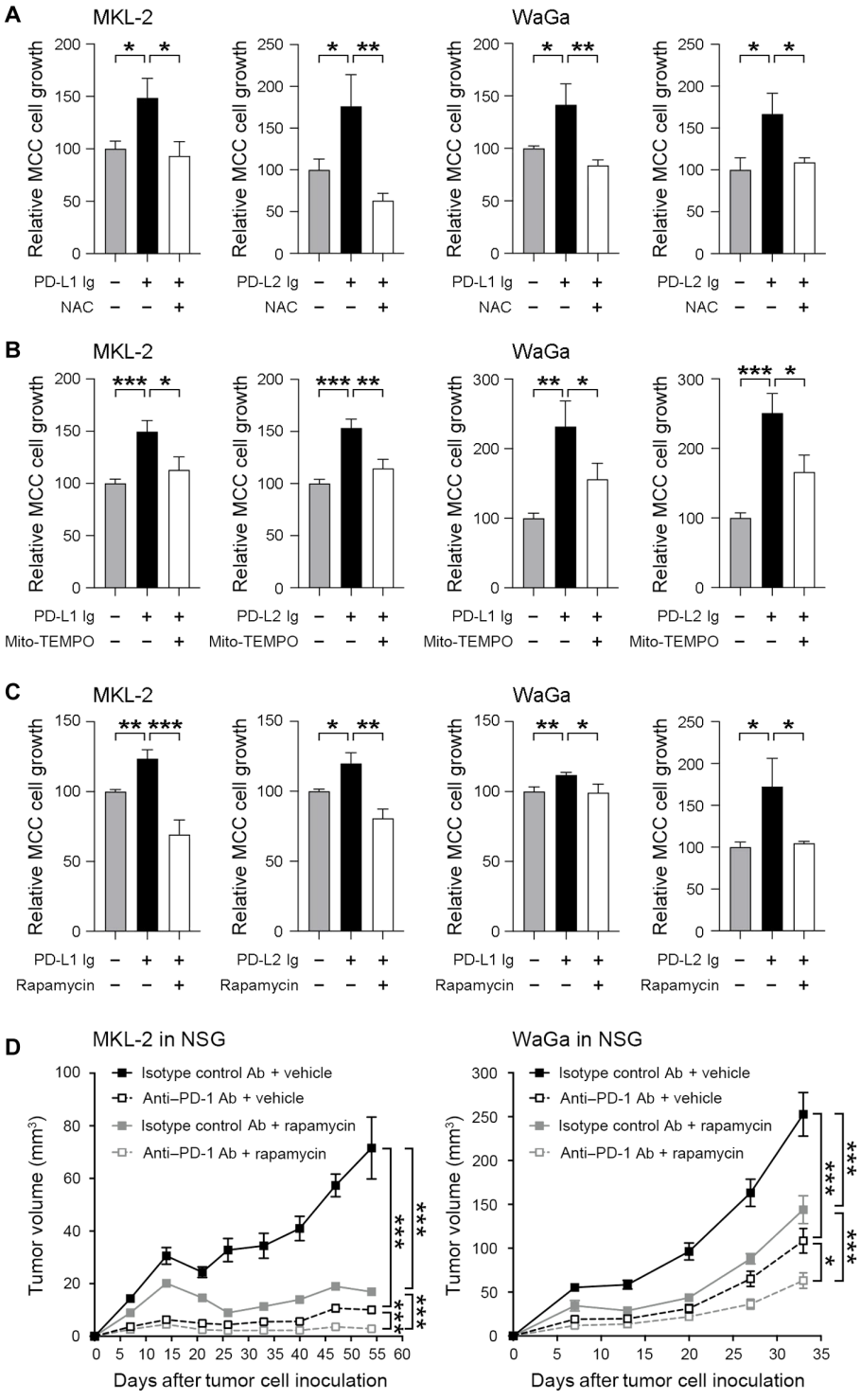

Fig. 6. MCC–PD-1–dependent growth requires mTOR signaling and mitochondrial ROS. Relative MCC tumor cell growth (means ± SEM) of MKL-2 (left) or WaGa (right) cultures treated with PD-L1 Ig (left) or PD-L2 Ig (right) versus control Ig, with or without (**A**) NAC, (**B**) mito-TEMPO, or (**C**) rapamycin versus respective vehicle control, as determined by CellTiter-Glo–based luminescence analysis. Results are representative of at least $n = 3$ independent experiments each. The control Ig groups were acquired concurrently with PD-L1 Ig and PD-L2 Ig treatment and are thus identical for some cell lines. (**D**) Tumor growth kinetics (means ± SEM) of MKL-2 or WaGa cells grafted to NSG mice treated with anti-human PD-1 blocking (nivolumab) versus isotype-matched control Ab with or without concurrent administration of rapamycin or vehicle control ($n = 8$ mice per experimental group). *$P < 0.05$; **$P < 0.01$; ***$P < 0.001$. See also fig. S6.

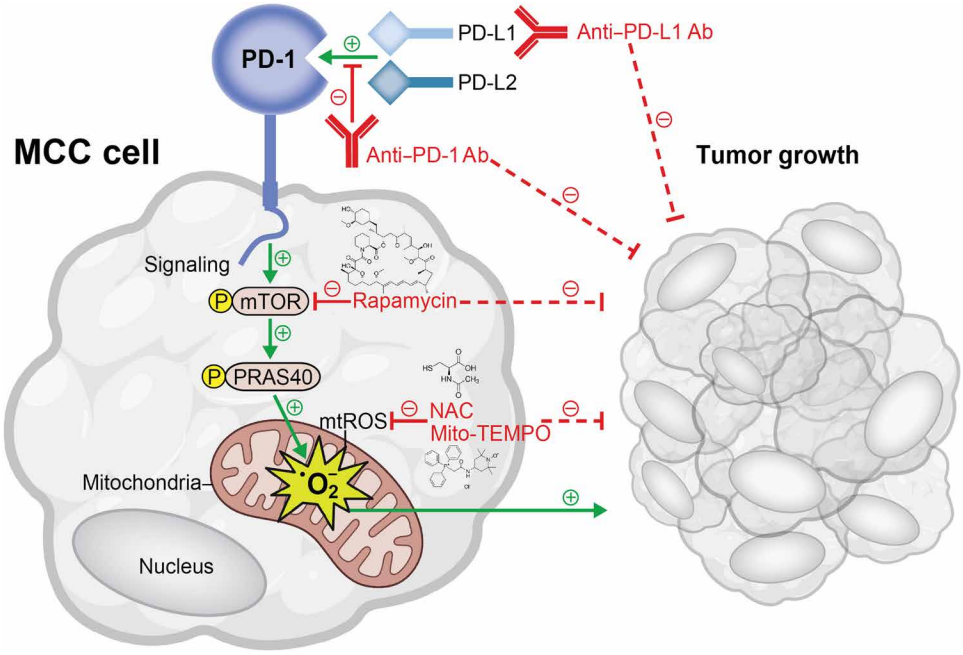

Fig. 7. The MCC-intrinsic PD-1 signaling axis promotes tumor growth. The MCC–PD-1 receptor binds PD-L1 and PD-L2 to activate (green, solid arrows) downstream mTOR and PRAS40 signaling and stimulate mtROS generation, facilitating MCC proliferation and growth. Ab-based blockade of MCC–PD-1 or PD-L1 or inhibition (red, solid lines) of mTOR (by rapamycin) or mtROS (by NAC or Mito-TEMPO) reverses (red, dashed lines) MCC–PD-1:PD-L1–dependent tumorigenesis. These findings identify a tumor cell–intrinsic mechanism through which PD-1 checkpoint antagonism might suppress MCC progression. Created with BioRender.com.

type. While tumor cell–PD-1 activates mTOR, PI3K, and/or MAPK signaling pathways in melanoma and other malignancies as reported by us and others (*17*, *18*, *23*, *26*, *27*, *34*, *35*), the functional involvement of such pathways in cancer cell–PD-1–dependent growth remains unknown. In contrast to melanoma cells, MCC cells did not show constitutive phosphorylation of the MAPK or PI3K/AKT/mTOR effectors, ERK1/2, AKT, or S6, consistent with the absence of melanoma-associated oncogenic driver mutations (*45*) in MCC (*46*). However, MCC cells at baseline demonstrated activation of the mTOR signaling mediators, mTOR and PRAS40. MCC–PD-1 ligation with either PD-L1 or PD-L2 induced, while nivolumab-based PD-1 blockade inhibited, phosphorylation of these mTOR effector molecules as well as downstream mtROS production and mitochondrial respiration. These findings identify a previously unknown protumorigenic, cancer cell–intrinsic PD-1 signaling circuit, mTOR-PRAS40-mtROS, the inhibition of which antagonizes MCC–PD-1–dependent tumorigenesis. While induction of mtROS via mTOR/PRAS40 is consistent with previous reports (*36*), this is the first demonstration linking oxidative metabolism to PD-1 receptor signaling in cancer cells.

In T cells, PD-1 ligation induces cytoplasmic but not mtROS production (*47*), of which the former is known to trigger apoptosis (*48*), consistent with the immune inhibitory role of the T cell–PD-1 checkpoint protein (*4*). In contrast, MCC–PD-1 elicited pro-proliferative as opposed to pro-apoptotic activity via mtROS but did not induce cytoplasmic ROS. mtROS in cancer cells is generally associated with tumor initiation, progression, and oncogenic pathway activation (*38*), including mTOR (*36*, *49*), and also induces PD-L1 expression (*50*, *51*). Our findings of MCC–PD-1:PD-L1–triggered tumor growth are thus consistent with such an mtROS-mTOR-PD-L1 circuit. In addition to modulating mitochondrial respiration, T cell–PD-1 ligation has also been found to attenuate glycolysis and promote functional exhaustion (*52*, *53*). On the other hand, we found that MCC–PD-1 interactions did not stimulate glycolysis or glucose uptake. These cell-type–dependent differences in PD-1–associated glucose metabolism underscore lineage complexities in PD-1 pathway functions that require further study.

Our findings using FDA-approved PD-1 checkpoint and pharmacologic inhibitors targeting the downstream mTOR-mtROS axis raise several considerations for clinical translation. For instance, mTOR antagonism with rapamycin reversed MCC–PD-1–dependent mitochondrial respiration and resultant proliferation and also synergized with PD-1 checkpoint therapy in suppressing tumorigenesis, thus highlighting the potential promise of mTOR-PD-1 combination drug regimens to thwart tumor cell–intrinsic PD-1 pro-growth effects. In further support, mTOR inhibition suppressed tumor cell–PD-1–dependent hepatocellular carcinoma growth (*27*). It also improved efficacy of PD-1 immunotherapy by enhancing T cell responses during the expansion phase (*54*). One concern is that mTOR inhibition can antagonize T effector cell immunity (*55*), especially during states of functional T cell exhaustion (*54*), thereby interfering with PD-1 ICI benefit. Hence, mTOR inhibitory strategies could be designed to specifically target expanding T cells and, in light of our findings, MCC cells to optimize ICI outcomes. Similar cell-type–dependent considerations also apply to agents targeting mtROS, the blockade of which using the growth inhibitory antioxidants, NAC or mito-TEMPO, reversed MCC–PD-1–dependent tumorigenesis. These results are consistent with the tumor growth–inhibitory effect of NAC- and mito-TEMPO–mediated mtROS antagonism in some malignancies (*56*–*58*). In the case of T cells, elevation of mtROS levels is desirable as it boosts proliferation and enhances PD-1 ICI response (*59*). This argues in favor of cell-type–directed therapeutic strategies that inhibit MCC cell–intrinsic mtROS to block

proliferation versus T cell–specific mtROS stimulation to enhance T cell immunity and improve ICI response.

In conclusion, we identify PD-1 as an MCC-intrinsic receptor that promotes tumorigenesis via downstream mTOR:PRAS40:mtROS signaling. Therapeutic targeting of the MCC–PD-1:PD-L1 axis and its downstream effectors, including with FDA-approved inhibitors of PD-1, mTOR, or mtROS, disrupts MCC growth. These results provide an additional layer of complexity to PD-1 pathway functions in distinct cell lineages and particularly in MCC cells. It also provides insight for both interpreting and optimizing ICI responses in this malignancy and potentially others. Accordingly, therapeutic regimens that optimally stimulate T cell antitumor activity and inhibit MCC–PD-1 protumorigenic processes such as mTOR and/or mtROS might improve PD-1 ICI–based MCC patient outcomes.

MATERIALS AND METHODS

MCC lines and clinical specimens, T cell and DC isolation, and culture methods

Authenticated, mycoplasma-free human A375 (catalog no. CRL-1619, RRID:CVCL_0132) and murine B16-F10 (catalog no. CRL-6475, RRID:CVCL_0159) melanoma cells were purchased from American Type Culture Collection (Gaithersburg, MD) and cultured as described (*18*, *40*). The human MCC cell lines, MKL-1 (RRID:CVCL_2600), MKL-2 (RRID:CVCL_D027), MS-1 (RRID:CVCL_E995), and WaGa (RRID:CVCL_E998), were obtained and cultured in RPMI 1640 medium (Life Technologies, Carlsbad, CA) supplemented with 20% (v/v) fetal bovine serum (FBS; Sigma-Aldrich, Saint Louis, MO) and 1% (v/v) penicillin/streptomycin (Life Technologies), as described (*32*). Immortalized normal telomerase reverse transcriptase (N/TERT-1) human keratinocytes (RRID:CVCL_CW92) were grown in keratinocyte serum–free medium supplemented with bovine pituitary extract (25 μg/ml), calcium dichloride (0.4 mM), epidermal growth factor (0.2 ng/ml), and penicillin/streptomycin [1% (v/v), Life Technologies], as described (*60*). All cell lines were used at low passage and <70% confluency. Single-cell suspensions were generated from human MCC tumor biospecimens using collagenase digestion, as described previously (*18*). Human peripheral blood mononuclear cells (PBMCs) were obtained from healthy donors, as described (*61*). T cells and monocytes were purified from these PBMC isolates using the RosetteSep Human T cell Enrichment Cocktail (STEMCELL Technologies, Vancouver, Canada) or CD14 microbeads (catalog no. 130-050-201, RRID:AB_2665482, Miltenyi Biotec, Gaithersburg, MD), respectively (*18*, *62*). T cells were resuspended at 1×10^6 to 3×10^6 cells/ml in advanced RPMI 1640 medium supplemented with 1% penicillin/streptomycin, 1% GlutaMAX 10×, 10 mM Hepes (Thermo Fisher Scientific, Waltham, MA), 10% FBS, recombinant human (rh) IL-2 (0.02 μg/ml; catalog no. 589104, BioLegend, San Diego, CA), and ImmunoCult human CD3/CD28 T cell activator (25 μL/ml; catalog no. 10971 or 10991, RRID:AB_2827806, STEMCELL Technologies) and cultured for 2 to 3 days before subsequent study. Monocytes were resuspended at 1×10^6 cells/ml and cultured for 6 days in advanced RPMI 1640 medium supplemented with 10% FBS, 1% penicillin/streptomycin, 2 mM GlutaMAX 10×, recombinant IL-4 (1000 U/ml; catalog no. 574002, BioLegend), and granulocyte-macrophage colony-stimulating factor (catalog no. 7954-GM-050/CF, R&D Systems, Minneapolis, MN) to generate dendritic cells (DCs). Murine splenocytes were isolated by mechanical disruption of mouse spleens derived from female C57BL/6 mice (RRID:IMSR_JAX:000664, the Jackson Laboratory, Bar Harbor, ME), as described (*63*). Briefly, splenocytes were resuspended at 1×10^6 cells/ml in advanced RPMI 1640 medium containing 1% penicillin/streptomycin, 1% GlutaMAX, 10 mM Hepes, 10% heat-inactivated FBS, recombinant mouse IL-2 (30 U/ml; BioLegend), and soluble anti-mouse CD28 Ab (2 μg/ml; catalog no. 553294, RRID:AB_394763, clone 37.51, BD Biosciences, Franklin Lakes, NJ) and seeded in 96-well plates (Corning, Glendale, AZ) pre-coated with anti-mouse CD3 Ab (10 μg/ml; catalog no. 553057, RRID:AB_394590, clone 145-2C11, BD Biosciences). Splenocytes were activated for 5 days before flow cytometric analyses. MCC biospecimens were obtained from patients, and blood from healthy volunteers, in accordance with protocols approved by the Institutional Review Boards (IRBs) of Mass General Brigham under protocol numbers 2022P002062, 2022P000827, and 2013P001014, respectively. Informed consent was obtained from all subjects, and all studies were conducted in accordance with the Declaration of Helsinki.

Generation of stable *PDCD1* KD MCC lines

Because MCC suspension cultures are challenging to transduce and chemically select, we developed a fluorescence-based cell sorting approach that avoids antibiotic selection and facilitates highly efficient gene KD. Specifically, single-stranded DNA constructs of 100 bases were synthesized encoding shRNA sequences targeting either human PD-1 (*PDCD1*, NM_005018.3) or a scrambled, nontargeting shRNA control (Life Technologies). Both DNA templates, which contained Eco RI and Pac I restriction sites flanking respective shRNA motifs, were PCR-amplified using the Platinum PCR SuperMix High Fidelity Kit (Invitrogen, Waltham, MA). Products were digested with Eco RI and Pac I (New England Biolabs, Ipswich, MA), purified using the MinElute Gel Extraction Kit (Qiagen, Beverly, MA), and ligated into the pLKO.3G lentiviral vector (catalog no. 14748, Addgene, Watertown, MA) encoding enhanced green fluorescent protein (EGFP) using the Rapid DNA Ligation Kit (Sigma-Aldrich), and sequences were validated by Sanger sequencing at the Dana-Farber/Harvard Cancer Center DNA Resource Core (Boston, MA). The target 21-mer, as previously described (*18*), was 5′-GCCTAGAGAAGTTTCAGGGAA-3′ (shRNA, human *PDCD1*) and 5′-GCGCGATAGCGCTAATAATTT-3′ (shRNA, scrambled control). Respective shRNAs were packaged into lentiviral particles by human embryonic kidney–293 Epstein-Barr virus nuclear antigen (EBNA) packaging cells (RRID:CVCL_6974) cotransfected with the viral packaging plasmids pN8e-GagPolΔ8.1 and pN8e-VSV-g, and viral supernatants were harvested 48 to 72 hours after transfection and filtered as described (*18*). MCC lines were stably transduced and flow cytometrically sorted to >95% purity for EGFP expression at the Beth Israel Deaconess Medical Center Flow Cytometry Core (Boston, MA). Robust KD of *PDCD1* was confirmed by RT-qPCR, immunoblotting, and flow cytometry.

Abs and biologic reagents

The following Abs and reagents were used for FACS analysis: PerCP-eFluor710–anti-human PD-1 Ab (clone MIH4, catalog no. 46-9969-42, RRID:AB_11219075) or PerCP-eFluor710-mouse IgG1 isotype control Ab (clone P3.6.2.8.1, catalog no. 46-4714-82, RRID:AB_1834453, eBiosciences, San Diego, CA), fluorescein isothiocyanate (FITC)–conjugated anti-human IgG4 (hIgG4; clone HP6023, catalog no. ab99815,

RRID:AB_10673905, Abcam, Cambridge, MA), phycoerythrin (PE)–conjugated anti-human PD-1 (clone J116, catalog no. NBP1-43107PE, Novus Biologicals, Littleton, CO) or anti-hIgG4 (clone HP6023, catalog no. ab99819, RRID:AB_10712191, Abcam), allophycocyanin (APC)–conjugated anti-human PD-1 (clone J116, catalog no. NBP143107J, Novus Biologicals), FITC-conjugated anti--human CD45 (clone HI30, catalog no. 304006, RRID:AB_314394) or mouse IgG1 isotype control Ab (clone MOPC-21, catalog no. 400110, RRID:AB_2861401), PE-conjugated anti-human PD-L1 (clone 29E.2A3, catalog no. 329706, RRID:AB_940368) or PD-L2 (clone 24F.10C12, catalog no.329606, RRID:AB_1089019), PE-conjugated mouse IgG1 (clone MOPC-21, catalog no. 400112, RRID:AB_2847829), mouse IgG2a (clone MOPC-173, catalog no. 400214, RRID:AB_2800438) or mouse IgG2b (clone MPC-11, catalog no. 400314, RRID:AB_2894969), APC-conjugated anti-human PD-L2 (clone 24F.10C12, catalog no. 329608, RRID:AB_1089013) or anti-mouse PD-L1 (clone 10F.9G2, catalog no. 124312, RRID:AB_10612741), APC-conjugated mouse IgG1 (clone MOPC-21, catalog no. 400122, RRID:AB_326443), mouse IgG2a (clone MOPC-173, catalog no. 400222, RRID:AB_2891178) or rat IgG2b (clone RTK4530, catalog no. 400612, RRID:AB_326556), PE-cyacine 7 (Cy7)–conjugated anti-human CD56 (clone 5.1H11, catalog no. 362510, RRID:AB_2563927), anti-human CD3 (clone HIT3a, catalog no. 300316, RRID:AB_314052), anti-mouse CD3 (clone 17A2, catalog no. 100220, RRID:AB_1732057), mouse IgG1 (clone MOPC-21, catalog no. 400126, RRID:AB_326448), mouse IgG2a (clone MOPC-173, catalog no. 400232, RRID:AB_326480) or rat IgG2b (clone RTK4530, catalog no. 400617, RRID:AB_326559), Brilliant Violet 605–conjugated anti-human PD-L1 (clone 29E.2A3, catalog no. 329724, RRID:AB_2565926) or mouse IgG2b (clone MPC-11, catalog no. 400350), Brilliant Violet 421–conjugated anti-human PD-L2 (clone 24F.10C12, catalog no. 329616, RRID:AB_2716087) or mouse IgG2a (clone MOPC-173, catalog no. 400260, RRID:AB_10960144), Spark Violet 538–conjugated anti-human CD3 (clone UCHT1, catalog no. 300484, RRID:AB_2890733) or mouse IgG1 (clone MOPC-21, catalog no. 402418), PE/Dazzle 594–conjugated anti-human CD45 (clone HI30, catalog no. 304052, RRID:AB_2563568) or mouse IgG1 (clone MOPC-21, catalog no. 400176, RRID:AB_2923261), Zombie NIR Fixable Viability Kit, Human TruStain FcX Receptor Blocking Solution (catalog no. 422302 or 422301, RRID:AB_2818986), TruStain FcX PLUS (anti-mouse CD16/32) Ab (catalog no. 156603 or 156604, RRID:AB_2783137), APC annexin V Apoptosis Detection Kit (catalog no. 640932) (all from BioLegend), CM-H2DCFDA (2′,7′-dichlorohydrofluorescein, catalog no. C6827), MitoSOX Red (mitohydroethidium, catalog no. M36008), MitoTracker Deep Red FM (catalog no. M46753), 4′,6-diamidino-2-phenylindole (DAPI) dyes (catalog no. 62247) (all from Life Technologies), and 2-NBDG Glucose Uptake Assay Kit (catalog no. AB235976, Abcam).

The following reagents were used for immunoblotting: unconjugated mouse anti-human PD-1 (1 μg/ml, clone J105, catalog no. 14-2799-95, RRID:AB_2865050, eBiosciences), mouse anti-human PD-1 (1 μg/ml, clone NAT105, catalog no. ab52587, RRID:AB_881954, Abcam), mouse anti-actin (1:2500 dilution, clone C4, catalog no. 612657, RRID:AB_399901, BD Biosciences), rabbit anti–phospho (p) mTOR (Ser^{2448}, clone D9C2, catalog no. 5536S, RRID:AB_10691552) and total (t-) mTOR (clone 7C10, catalog no. 2983S, RRID:AB_2105622), rabbit anti–p-PRAS40 (Thr^{246}, clone C77D7, catalog no. 2997S, RRID:AB_2258110) and t-PRAS40 (clone D23C7, catalog no. 2691S, RRID:AB_2225033), rabbit anti–p-Akt (Ser^{473}, clone D9E, catalog no. 4060S, RRID:AB_2315049) and t-Akt (clone C67E7, catalog no. 4691S, RRID:AB_915783), rabbit anti–p-S6 (Ser$^{235/236}$, clone 91B2, catalog no. 4857S, RRID:AB_2181035) and t-S6 (clone 5G10, catalog no. 2217S, RRID:AB_331355), rabbit anti–p-ERK1/2 (Thr^{202}/Tyr^{204}, clone D13.14.4E, 4370S, RRID:AB_2315112) and t-ERK1/2 (clone 137F5, catalog no. 4695S, RRID:AB_390779) (all used at 1:500 to 1:2000 dilution, Cell Signaling Technology, Danvers, MA), horseradish peroxidase (HRP)–conjugated goat anti-mouse (catalog no. 1010-05, RRID: AB_2728714) or goat anti-rabbit IgG Ab (catalog no. 4050-05, RRID:AB_2795955) (all from SouthernBiotech, Birmingham, AL), and goat anti-rabbit IgG Ab (catalog no. 7074S, Cell Signaling Technology), all used at 1:2000 or 1:5000 dilution.

The following Abs and/or reagents were used for IF staining: unconjugated rabbit anti-human PD-1 (1:20, clone D4WZJ, catalog no. 86163S, RRID:AB_2728833, Cell Signaling Technology), biotin-conjugated goat anti-rabbit IgG (1:200, catalog no. BA-100, Vector Laboratories, Burlingame, CA), streptavidin-Cy5 (1:50, catalog no. 434316, Life Technologies), rabbit anti-human CK20 (1:200, clone D9Z1Z, catalog no. 13063S, RRID:AB_2798106, Cell Signaling Technology), mouse anti-human CD45 (1:100, clone MEM-28, catalog no. ab8216, RRID:AB_306361, Abcam), Cy3-conjugated goat anti-rabbit IgG (1:2000, catalog no. A10520, RRID:AB_2534029, Thermo Fisher Scientific), Alexa Fluor 488 (AF488)–conjugated goat anti-mouse IgG1 (1:2000, catalog no. A-11001 (also A11001, A 11001), RRID:AB_2534069, Thermo Fisher Scientific), and ProLong Glass Antifade Mountant with NucBlue Stain (catalog no. P36983, Life Technologies).

The following proteins and reagents were used for assessment of tumor cell proliferation and growth, metabolism, and signaling: rh-PD-L1 (B7-H1, catalog no. 156-B7-100), PD-L2 (B7-DC, catalog no. 1224-PL-100), or IgG1 control Fc chimera proteins (catalog no. 110-HG-100, R&D Systems); anti–PD-1 Abs, nivolumab (Opdivo, Bristol Myers Squibb, New York, NY), and J116 (catalog no. BE0188, RRID:AB_10950318, Bio X Cell, Lebanon, NH); anti-human PD-L1 (clone 29E.2A3, catalog no. 329746, RRID:AB_2783199, BioLegend); anti-mouse PD-L1 (clone 10F.9G2, catalog no. 124339, RRID:AB_2800597, BioLegend); ultra-LEAF hIgG4 (catalog no. 403702, BioLegend); mouse IgG2b (clone MPC-11, catalog no. 400370, BioLegend); ultra-LEAF rat IgG2b (clone RTK4530, catalog no. 400672, BioLegend) or mouse IgG1 isotype control Abs (clone MOPC-21, catalog no. BE0083, RRID:AB_1107784, Bio X Cell). Rapamycin (catalog no. S1039), mito-TEMPO (catalog no. S9733), and *N*-acetylcysteine (NAC; catalog no. S1623) were purchased from Selleckchem (Houston, TX).

RT-PCR and RT-qPCR

Total RNA was extracted from cell lines and tumor xenografts using the RNeasy Plus Mini Kit (catalog no. 74134, Qiagen, Germantown, MD), according to the manufacturer's protocol, as described (*18*, *39*, *61*). For RT-qPCR analyses, RNA was converted to cDNA using the SuperScript VILO cDNA synthesis kit (catalog no. 11754050, Thermo Fisher Scientific), and samples were assayed in triplicate using the Fast SYBR Green Master Mix (catalog no. 4385612, Thermo Fisher Scientific) with primer sets, as below, on a QuantStudio 5 Real-Time PCR system (Applied Biosystems, Waltham, MA). Thermal cycling was carried out at 94°C for 2 min, followed by 40 cycles at 94°C for 15 s, 60°C for 20 s, and 68°C for 1 min, as described, followed by melt-curve analysis. Data were normalized to human 18*S* ribosomal RNA (rRNA), and relative transcript levels were calculated

using the delta-delta threshold cycle (Ct) method (*18*, *39*, *61*). Samples with Ct numbers above the water negative control or those with more than one melt curve were designated as not detected. The primer sequences used for human *PDCD1* were (forward) 5′-GACAGCGGCACCTACCTCTGTG-3′ and (reverse) 5′-GACCCAGACTAGCAGCACCAGG-3′, for human *PDCD1LG1* were (forward) 5′-TGCCGACTACAAGCGAATTACT-3′ and (reverse) 5′-CTGCTTGTCCA GATGACTTCGG-3′, for human *PDCD1LG2* were (forward) 5′-CTCGTTCCACATACCTCAAGTCC-3′ and (reverse) 5′-CTGGAACCTTTAGGATGTGAGTG-3′, and for human 18*S* rRNA were (forward) 5′-GATGGGCGGCGGAAAATAG-3′ and (reverse) 5′-GCGTGGATTCTGCATAATGGT-3′. For RT-PCR–based sequencing of the full human *PDCD1* coding sequence (NM_005018.3), reverse-transcribed products were amplified with the Platinum PCR SuperMix High Fidelity Kit (catalog no. 12532016, Life Technologies) using the following primer pair: (forward) 5′-ATGCAGATCCCACAGGCGCC-3′ and (reverse) 5′-TCAGAGGGGCCAAGAGCAGTG-3′. PCR-amplified human *GAPDH*, (forward) 5′-ACCACAGTCCATGCCATCAC-3′ and (reverse) 5′-TCCACCACCCTGTTGCTGTA-3′, was used as a loading control. Thermocycling was carried out at 94°C for 2 min, followed by 40 cycles at 94°C for 15 s, 60°C for 20 s, and 68°C for 1 min. The 867-base *PDCD1* PCR products were resolved by agarose (1%) gel electrophoresis, images were acquired on an Alpha Innotech Multilmage Light Cabinet (Alpha Innotech, San Jose, CA), bands were extracted, and DNA was isolated, as described (*18*, *61*). The full coding sequences of MCC cell line–expressed *PDCD1* (NM_005018.3) were submitted to the GenBank database under the following accession numbers: MKL-1 (OQ594425), MKL-2 (OQ594426), MS-1 (OQ594427), and WaGa (OQ594428).

Flow cytometry

PD-1 surface protein expression by human MCC lines, cell suspensions derived from MCC tumor xenografts, or MCC patient specimens as well as by human T cells, A375 melanoma cells, immortalized N/TERT-1 keratinocytes and murine splenocytes, and B16-F10 melanoma cells was analyzed by multicolor flow cytometry, as described (*18*, *39*, *61*). To exclude dead cells, staining with the Zombie NIR Fixable Viability Kit (1:1000) was performed for 10 min at room temperature in the dark, following the manufacturer's recommendations. Cells were then blocked with the Human TruStain FcX Receptor Blocking Solution for 10 min at room temperature and then stained with fluorochrome-conjugated Abs (20 μg/ml), as described (*18*, *39*, *61*), or with nivolumab (100 μg/ml) in PBS + 2% (v/v) FBS, for 30 min at 4°C, followed by subsequent washing. Nivolumab binding was detected using FITC-conjugated anti-hIgG4. Isotype control Abs were used, and cell doublets were excluded for all analyses. Because MIH4 Ab reactivity varied on the basis of fluorophore and detection equipment, all matched comparisons used identical staining approaches and flow cytometric imagers. Cell death was also measured with the APC Annexin V Apoptosis Detection Kit (BioLegend), as described (*40*). For ROS quantification, cells were incubated for 15 min at 37°C with CM-H2DCFDA, MitoSOX Red, MitoTracker Deep Red FM, and/or DAPI dyes, as described (*59*, *64*). For glucose uptake assays, cells in glucose-free RPMI medium were incubated with 2-NBDG (100 μg/ml) for 10 min and then counterstained with PI according to the manufacturer's instructions. Fluorescence emission was acquired on a FacsCanto (BD Biosciences) or an Aurora Spectral Viewer (RRID:SCR_019826, Cytek, Fremont, CA), and data were analyzed using FlowJo version 10.8.1 (RRID:SCR_008520, TreeStar, Ashland, OR).

Immunoblotting

Cells were lysed in ice-cold radioimmunoprecipitation assay buffer supplemented with Pierce Protease and Phosphatase Inhibitor Mini Tablets, EDTA-free (catalog no. A32961) or Halt Phosphatase Inhibitor Cocktail and Halt Protease Inhibitor Cocktail (100×) (catalog no. 78440, Thermo Fisher Scientific) or Protease/Phosphatase Inhibitor Cocktail (100×, catalog no. 5872S, Cell Signaling Technology) and vortexed at 4°C for 30 min, as described (*18*, *61*). Protein concentrations were determined using the Pierce BCA Protein Assay Kit (catalog no.23225, Thermo Fisher Scientific), according to the manufacturer's protocol. Total proteins were resolved in 7.5% or 4 to 15% SDS–polyacrylamide gel electrophoresis gels and transferred to Sequi-Blot PVDF membranes (Bio-Rad, Hercules, CA). Membranes were blocked in tris-buffered saline (TBS)/0.1% (v/v) Tween 20 (Sigma-Aldrich, -T), containing 5% (w/v) bovine serum albumin (Sigma-Aldrich or Cell Signaling Technology) for at least 1 hour at room temperature, and then incubated overnight at 4°C with primary Ab. Subsequently, blots were washed thrice in TBS-T and incubated with secondary HRP-conjugated Ab for 1 hour at room temperature. Antigens were visualized using the Lumi-Light Western blotting substrate (Roche, Indianapolis, IN) on HyBlot CL Autoradiography Films (Thomas Scientific, Swedesboro, NJ) using a Kodak Min-R mammography processor (Kodak, Rochester, NY). For detection of actin and total proteins, blots were stripped with the Restore Western blot Stripping Buffer (Thermo Fisher Scientific) according to the manufacturer's protocol, blocked, and incubated overnight at 4°C with primary Ab and then with secondary HRP-conjugated Ab for 1 hour at room temperature. Expression levels of p-mTOR and p-PRAS40 versus respective t-controls were determined in MKL-1, MKL-2, MS-1, and WaGa cells, as described (*61*). Briefly, MCC cells were cultured in growth medium without serum for 12 hours at 37°C and then stimulated with rhPD-L1 or rhPD-L2 (20 μg/ml) or hIgG1 for 24 hours (MKL-1), 36 hours (MKL-2 and MS-1), or 12 hours (WaGa) at 37°C, followed by lysate generation. For Ab treatment groups, MCC lines were stimulated for 1 hour at 37°C with nivolumab (100 μg/ml) or respective isotype control Ab in growth medium without serum before stimulation with rhPD-L1, rhPD-L2, or hIgG1 (20 μg/ml).

IF staining

PD-1/CK20/CD45 IF triple labeling of clinical MCC patient specimens ($n = 13$) was carried out as described previously (*18*, *32*, *61*). Briefly, formalin-fixed, paraffin-embedded sections were baked for 30 min at 56°C, deparaffinized in xylene for 10 min, and rehydrated with successive 2 min baths of 100, 95, and 75% (v/v) ethanol. Sections were then submerged in a Target Antigen Retrieval solution (pH 6.0; Dako, Carpinteria, CA) and pressure-cooked in a decloaking chamber (Biocare Medical, Pacheco, CA) at 110°C for 15 min to retrieve antigens. Subsequently, sections were blocked with 10% (v/v) goat, avidin-blocking, and biotin-blocking sera (Vector Laboratories) and lastly incubated with anti-human PD-1 Ab (1:20 dilution) at 4°C overnight. Sections were washed thrice with TBS-T for 5 min, incubated for 1 hour at room temperature with biotin-conjugated goat anti-rabbit IgG (1:200), washed three times, and incubated at room temperature for 1 hour with strepatividin-Cy5 (1:50). After blocking with 10% goat serum, sections were incubated

with rabbit anti-human CK20 and mouse anti-human CD45 (1:200 and 1:100, respectively) at 4°C overnight. After blocking with 0.1% (v/v) Sudan Black B solution (Sigma-Aldrich) and rinsing with TBS-T, sections were incubated for 1 hour at room temperature with Cy3-conjugated goat anti-rabbit IgG and AF488-conjugated goat anti-mouse IgG1 (1:2000) and mounted with ProLong Glass Antifade Mountant with NucBlue Stain (Thermo Fisher Scientific). IF was analyzed on an EVOS FL Auto 2 Imaging system microscope (Thermo Fisher Scientific). Images were processed using ImageJ (National Institutes of Health, Bethesda, MD).

Cell proliferation assays

MCC cell proliferation was assessed via the Promega CellTiter-Glo2.0 Assay (catalog no. G9242, Promega, Madison, WI), according to the manufacturer's instructions, using a Promega GloMAX 96 microplate luminometer. To that end, cells were seeded in 96-well microplates with white flat bottoms (Corning, Corning, NY), treated with nivolumab (100 μg/ml) versus hIgG4 control Abs with or without anti-human PD-L1 or mouse IgG2b Abs (100 μg/ml) for 5 days or rhPD-L1, rhPD-L2, or hIgG1 (20 μg/ml) for 3 days, following pretreatment with or without 50 nM rapamycin (30 min), 0.1 μM mito-TEMPO (2 hours), or 10 μM NAC (2 hours).

Metabolic profiling

OCRs and ECARs of MCC cells were measured using the Seahorse XFe96 Analyzer (Agilent Technologies, Santa Clara, CA), according to the manufacturer's guidelines. Specifically, MCC cells were plated in 96-well Seahorse XF96 cell culture microplates (catalog no. 102601-100, Agilent) coated with Corning Cell-Tak Cell and Tissue Adhesive (22.4 μg/ml; catalog no. CB40240, Corning) in RPMI without L-glutamine with 1% penicillin/streptomycin (Life Technologies). Cells were starved overnight and then stimulated for 24 hours with rhPD-L1, rhPD-L2, or hIgG1 (20 μg/ml) in the presence or absence of nivolumab (100 μg/ml) or respective isotype control Abs, with or without rapamycin (10 to 50 nM), 0.1 μM mito-TEMPO, or 10 μM NAC. Measurements of OCR were performed, as described (*64*), after sequential injections of 10 mM oligomycin [adenosine 5′-triphosphate (ATP) synthase inhibitor, catalog no. 75351-5mG], 100 mM 2,4-DNP (mitochondrial uncoupler, catalog no. D198501-5G), 10 mM rotenone (mitochondrial complex I inhibitor, catalog no. R8875-1G), and 10 mM antimycin A (mitochondrial complex III inhibitor, catalog no. A8674-100MG). ECAR changes were measured after three sequential injections of glucose (20 g/liter; catalog no. A2494001, Life Technologies), 10 mM oligomycin (ATP synthase inhibitor), and 50 mM 2-deoxy-glucose (Hexokinase inhibitor, catalog no. D8375-5G, Sigma-Aldrich), as described (*64*).

In vivo tumorigenicity studies

NOD/SCID/IL-2rγ$^{-/-}$ (NSG) mice (RRID: IMSR_JAX:005557) were purchased from the Jackson Laboratory, maintained, and housed at the Brigham and Women's Hospital (BWH) animal facility, as described (*18*, *32*, *61*). All mice were female, at least 6 weeks of age, and used in accordance with the National Institutes of Animal Healthcare Guidelines under the BWH Institutional Animal Care and Use Committee (IACUC)–approved experimental protocol 2016 N000112. The study is reported in accordance with Animal Research: Reporting of In Vivo Experiments (ARRIVE) guidelines. Human MCC cell lines were injected subcutaneously (1×10^7 cells per inoculum for MKL-1 wild-type, *PDCD1* KD, and scrambled shRNA control cells, MS-1, and WaGa; 5×10^6 cells per inoculum for WaGa *PDCD1* KD and scrambled shRNA control cells; and 1×10^6 cells per inoculum for MKL-2) into the flanks of recipient NSG mice, as described (*18*, *32*, *61*). Mice were randomly assigned to experimental groups and injected intraperitoneally with 200 μg of blocking anti-human PD-1 Ab clone J116 (MKL-1, MS-1, and WaGa) or nivolumab (MKL-2 and WaGa), anti-human PD-L1 Ab (Bio X Cell) clone 29E.2A3 (MKL-2, WaGa), anti-mouse PD-L1 Ab (Bio X Cell) clone 10F.9G2 (MKL-2, WaGa), or respective isotype control Abs, including mouse IgG1 clone MOPC-21, hIgG4 clone QA16A15, mouse IgG2b clone MPC-11, or rat IgG2b clone RTK4530 (all from BioLegend) every 3 days starting 1 day before tumor cell inoculation, with tumor formation/growth assessments by investigators not blinded to the experimental treatment, as described (*18*). For mTOR and ROS inhibition studies, mice were fed submaximal doses of either rapamycin (5 mg/kg per day) or NAC (200 mg/kg per day) along with vehicle control incorporated into rodent chow (Research Diet Inc.) or injected intraperitoneally with mito-TEMPO (1.25 mg/kg) or vehicle control every 2 days for the duration of experiments (*28*–*31*, *65*). In some experiments where indicated, mice were treated concurrently with both nivolumab and rapamycin, with nivolumab alone for the first 3 weeks followed by rapamycin alone, or with rapamycin alone for the first 3 weeks followed by nivolumab alone until the experimental endpoint. Tumors were harvested 5 to 10 weeks after tumor cell graftment unless excessive tumor size or disease state required protocol-stipulated euthanasia earlier. Sample sizes of at least $n = 6$ to 10 mice per experimental group were used on the basis of previous studies conducted by our laboratories that consistently yielded sufficient power to detect statistically significant differences (*18*).

Statistical analysis

Statistical differences between groups were compared using the unpaired Student's *t* test, the nonparametric Mann-Whitney test (comparison of two experimental groups), one-way analysis of variance (ANOVA) with Dunnett posttest, repeated-measures two-way ANOVA, or mixed model followed by the Bonferroni correction (comparison of three or more experimental groups). Data were tested for normal distribution using the D'Agostino and Pearson omnibus normality test. A two-tailed value of $P < 0.05$ was considered statistically significant (*18*, *32*, *61*). All statistical analyses were performed using the PRISM 10.0.2 software (RRID:SCR_002798, GraphPad, San Diego, CA).

Study approval

All studies involving human specimens were approved by the Mass General Brigham IRBs, under protocol numbers 2022P002062, 2022P000827, and 2013P001014. Written informed consent was obtained from all subjects, and all studies were conducted in accordance with the Declaration of Helsinki. All animal experiments were conducted under protocol number 2016 N000112 approved by the IACUC of BWH, Boston, MA.

Supplementary Materials

This PDF file includes:

Figs. S1 to S6

REFERENCES AND NOTES

1. P. Sharma, B. A. Siddiqui, S. Anandhan, S. S. Yadav, S. K. Subudhi, J. Gao, S. Goswami, J. P. Allison, The next decade of immune checkpoint therapy. *Cancer Discov.* **11**, 838–857 (2021).
2. G. J. Freeman, A. J. Long, Y. Iwai, K. Bourque, T. Chernova, H. Nishimura, L. J. Fitz, N. Malenkovich, T. Okazaki, M. C. Byrne, H. F. Horton, L. Fouser, L. Carter, V. Ling, M. R. Bowman, B. M. Carreno, M. Collins, C. R. Wood, T. Honjo, Engagement of the PD-1 immunoinhibitory receptor by a novel B7 family member leads to negative regulation of lymphocyte activation. *J. Exp. Med.* **192**, 1027–1034 (2000).
3. Y. Latchman, C. R. Wood, T. Chernova, D. Chaudhary, M. Borde, I. Chernova, Y. Iwai, A. J. Long, J. A. Brown, R. Nunes, E. A. Greenfield, K. Bourque, V. A. Boussiotis, L. L. Carter, B. M. Carreno, N. Malenkovich, H. Nishimura, T. Okazaki, T. Honjo, A. H. Sharpe, G. J. Freeman, PD-L2 is a second ligand for PD-1 and inhibits T cell activation. *Nat. Immunol.* **2**, 261–268 (2001).
4. A. H. Sharpe, K. E. Pauken, The diverse functions of the PD1 inhibitory pathway. *Nat. Rev. Immunol.* **18**, 153–167 (2018).
5. P. Georgiev, E. S. Muise, D. E. Linn, M. C. Hinton, Y. Wang, M. Cai, L. Cadzow, D. C. Wilson, S. Sukumar, M. Caniga, L. Chen, H. Xiao, J. H. Yearley, V. Sriram, M. Nebozhyn, M. Sathe, W. M. Blumenschein, K. S. Kerr, H. A. Hirsch, S. Javaid, A. K. Olow, L. Y. Moy, D. Y. Chiang, A. Loboda, R. Cristescu, S. Sadekova, B. J. Long, T. K. McClanahan, E. M. Pinheiro, Reverse translating molecular determinants of anti-programmed death 1 immunotherapy response in mouse syngeneic tumor models. *Mol. Cancer Ther.* **21**, 427–439 (2022).
6. V. R. Juneja, K. A. McGuire, R. T. Manguso, M. W. LaFleur, N. Collins, W. N. Haining, G. J. Freeman, A. H. Sharpe, PD-L1 on tumor cells is sufficient for immune evasion in immunogenic tumors and inhibits CD8 T cell cytotoxicity. *J. Exp. Med.* **214**, 895–904 (2017).
7. C. Robert, A decade of immune-checkpoint inhibitors in cancer therapy. *Nat. Commun.* **11**, 3801 (2020).
8. A. Kalbasi, A. Ribas, Tumour-intrinsic resistance to immune checkpoint blockade. *Nat. Rev. Immunol.* **20**, 25–39 (2020).
9. P. W. Harms, K. L. Harms, P. S. Moore, J. A. DeCaprio, P. Nghiem, M. K. K. Wong, I. Brownell; International Workshop on Merkel Cell Carcinoma Research (IWMCC) Working Group, The biology and treatment of Merkel cell carcinoma: Current understanding and research priorities. *Nat. Rev. Clin. Oncol.* **15**, 763–776 (2018).
10. P. T. Nghiem, S. Bhatia, E. J. Lipson, R. R. Kudchadkar, N. J. Miller, L. Annamalai, S. Berry, E. K. Chartash, A. Daud, S. P. Fling, P. A. Friedlander, H. M. Kluger, H. E. Kohrt, L. Lundgren, K. Margolin, A. Mitchell, T. Olencki, D. M. Pardoll, S. A. Reddy, E. M. Shantha, W. H. Sharfman, E. Sharon, L. R. Shemanski, M. M. Shinohara, J. C. Sunshine, J. M. Taube, J. A. Thompson, S. M. Townson, J. H. Yearley, S. L. Topalian, M. A. Cheever, PD-1 blockade with pembrolizumab in advanced Merkel-cell carcinoma. *N. Engl. J. Med.* **374**, 2542–2552 (2016).
11. K. G. Paulson, S. Y. Park, N. A. Vandeven, K. Lachance, H. Thomas, A. G. Chapuis, K. L. Harms, J. A. Thompson, S. Bhatia, A. Stang, P. Nghiem, Merkel cell carcinoma: Current US incidence and projected increases based on changing demographics. *J. Am. Acad. Dermatol.* **78**, 457–463.e2 (2018).
12. C. H. Kugel III, S. M. Douglass, M. R. Webster, A. Kaur, Q. Liu, X. Yin, S. A. Weiss, F. Darvishian, R. N. Al-Rohil, A. Ndoye, R. Behera, G. M. Alicea, B. L. Ecker, M. Fane, M. J. Allegrezza, N. Svoronos, V. Kumar, D. Y. Wang, R. Somasundaram, S. Hu-Lieskovan, A. Ozgun, M. Herlyn, J. R. Conejo-Garcia, D. Gabrilovich, E. L. Stone, T. S. Nowicki, J. Sosman, R. Rai, M. S. Carlino, G. V. Long, R. Marais, A. Ribas, Z. Eroglu, M. A. Davies, B. Schilling, D. Schadendorf, W. Xu, R. K. Amaravadi, A. M. Menzies, J. L. McQuade, D. B. Johnson, I. Osman, A. T. Weeraratna, Age correlates with response to anti-PD1, reflecting age-related differences in intratumoral effector and regulatory T-cell populations. *Clin. Cancer Res.* **24**, 5347–5356 (2018).
13. H. Feng, M. Shuda, Y. Chang, P. S. Moore, Clonal integration of a polyomavirus in human Merkel cell carcinoma. *Science* **319**, 1096–1100 (2008).
14. S. R. Gordon, R. L. Maute, B. W. Dulken, G. Hutter, B. M. George, M. N. McCracken, R. Gupta, J. M. Tsai, R. Sinha, D. Corey, A. M. Ring, A. J. Connolly, I. L. Weissman, PD-1 expression by tumour-associated macrophages inhibits phagocytosis and tumour immunity. *Nature* **545**, 495–499 (2017).
15. J. Hsu, J. J. Hodgins, M. Marathe, C. J. Nicolai, M. C. Bourgeois-Daigneault, T. N. Trevino, C. S. Azimi, A. K. Scheer, H. E. Randolph, T. W. Thompson, L. Zhang, A. Iannello, N. Mathur, K. E. Jardine, G. A. Kirn, J. C. Bell, M. W. McBurney, D. H. Raulet, M. Ardolino, Contribution of NK cells to immunotherapy mediated by PD-1/PD-L1 blockade. *J. Clin. Invest.* **128**, 4654–4668 (2018).
16. B. A. Helmink, S. M. Reddy, J. Gao, S. Zhang, R. Basar, R. Thakur, K. Yizhak, M. Sade-Feldman, J. Blando, G. Han, V. Gopalakrishnan, Y. Xi, H. Zhao, R. N. Amaria, H. A. Tawbi, A. P. Cogdill, W. Liu, V. S. LeBleu, F. G. Kugeratski, S. Patel, M. A. Davies, P. Hwu, J. E. Lee, J. E. Gershenwald, A. Lucci, R. Arora, S. Woodman, E. Z. Keung, P. O. Gaudreau, A. Reuben, C. N. Spencer, E. M. Burton, L. E. Haydu, A. J. Lazar, R. Zapassodi, C. W. Hudgens, D. A. Ledesma, S. Ong, M. Bailey, S. Warren, D. Rao, O. Krijgsman, E. A. Rozeman, D. Peeper, C. U. Blank, T. N. Schumacher, L. H. Butterfield, M. A. Zelazowska, K. M. McBride, R. Kalluri, J. Allison, F. Petitprez, W. H. Fridman, C. Sautes-Fridman, N. Hacohen, K. Rezvani, P. Sharma, M. T. Tetzlaff, L. Wang, J. A. Wargo, B cells and tertiary lymphoid structures promote immunotherapy response. *Nature* **577**, 549–555 (2020).
17. C. A. Clark, H. B. Gupta, G. Sareddy, S. Pandeswara, S. Lao, B. Yuan, J. M. Drerup, A. Padron, J. Conejo-Garcia, K. Murthy, Y. Liu, M. J. Turk, K. Thedieck, V. Hurez, R. Li, R. Vadlamudi, T. J. Curiel, Tumor-intrinsic PD-L1 signals regulate cell growth, pathogenesis, and autophagy in ovarian cancer and melanoma. *Cancer Res.* **76**, 6964–6974 (2016).
18. S. Kleffel, C. Posch, S. R. Barthel, H. Mueller, C. Schlapbach, E. Guenova, C. P. Elco, N. Lee, V. R. Juneja, Q. Zhan, C. G. Lian, R. Thomi, W. Hoetzenecker, A. Cozzio, R. Dummer, M. C. Mihm Jr., K. T. Flaherty, M. H. Frank, G. F. Murphy, A. H. Sharpe, T. S. Kupper, T. Schatton, Melanoma cell-intrinsic PD-1 receptor functions promote tumor growth. *Cell* **162**, 1242–1256 (2015).
19. S. Yang, J. Wei, Y. H. Cui, G. Park, P. Shah, Y. Deng, A. E. Aplin, Z. Lu, S. Hwang, C. He, Y. Y. He, m^6A mRNA demethylase FTO regulates melanoma tumorigenicity and response to anti-PD-1 blockade. *Nat. Commun.* **10**, 2782 (2019).
20. M. Sanlorenzo, I. Vujic, A. Floris, M. Novelli, L. Gammaitoni, L. Giraudo, M. Macagno, V. Leuci, R. Rotolo, C. Donini, M. Basirico, P. Quaglino, M. T. Fierro, S. Giordano, M. Sibilia, F. Carnevale-Schianca, M. Aglietta, D. Sangiolo, BRAF and MEK inhibitors increase PD-1-positive melanoma cells leading to a potential lymphocyte-independent synergism with anti-PD-1 antibody. *Clin. Cancer Res.* **24**, 3377–3385 (2018).
21. Z. Cao, N. Kon, Y. Liu, W. Xu, J. Wen, H. Yao, M. Zhang, Z. Wu, X. Yan, W. G. Zhu, W. Gu, D. Wang, An unexpected role for p53 in regulating cancer cell-intrinsic PD-1 by acetylation. *Sci. Adv.* **7**, (2021).
22. S. Du, N. McCall, K. Park, Q. Guan, P. Fontina, A. Ertel, T. Zhan, A. P. Dicker, B. Lu, Blockade of tumor-expressed PD-1 promotes lung cancer growth. *Onco. Targets. Ther.* **7**, e1408747 (2018).
23. C. Ierano, D. Righelli, C. D'Alterio, M. Napolitano, L. Portella, G. Rea, F. Auletta, S. Santagata, A. M. Trotta, G. Guardascione, F. Liotti, N. Prevete, P. Maiolino, A. Luciano, A. Barbieri, A. Di Mauro, C. Roma, R. Esposito Abate, F. Tatangelo, R. Pacelli, N. Normanno, R. M. Melillo, S. Scala, In PD-1+ human colon cancer cells NIVOLUMAB promotes survival and could protect tumor cells from conventional therapies. *J. Immunother. Cancer* **10**, e004032, e004032 (2022).
24. R. Mirzaei, A. Gordon, F. J. Zemp, M. Kumar, S. Sarkar, H. A. Luchman, A. C. Bellail, C. Hao, D. J. Mahoney, J. F. Dunn, P. Bose, V. W. Yong, PD-1 independent of PD-L1 ligation promotes glioblastoma growth through the NFκB pathway. *Sci. Adv.* **7**, eabh2148 (2021).
25. X. Wang, X. Yang, C. Zhang, Y. Wang, T. Cheng, L. Duan, Z. Tong, S. Tan, H. Zhang, P. E. Saw, Y. Gu, J. Wang, Y. Zhang, L. Shang, Y. Liu, S. Jiang, B. Yan, R. Li, Y. Yang, J. Yu, Y. Chen, G. F. Gao, Q. Ye, S. Gao, Tumor cell-intrinsic PD-1 receptor is a tumor suppressor and mediates resistance to PD-1 blockade therapy. *Proc. Natl. Acad. Sci.* **117**, 6640–6650 (2020).
26. C. D'Alterio, M. Buoncervello, C. Ierano, M. Napolitano, L. Portella, G. Rea, A. Barbieri, A. Luciano, G. Scognamiglio, F. Tatangelo, A. M. Anniciello, M. Monaco, E. Cavalcanti, P. Maiolino, G. Romagnoli, C. Arra, G. Botti, L. Gabriele, S. Scala, Targeting CXCR4 potentiates anti-PD-1 efficacy modifying the tumor microenvironment and inhibiting neoplastic PD-1. *J. Exp. Clin. Cancer Res.* **38**, 432 (2019).
27. H. Li, X. Li, S. Liu, L. Guo, B. Zhang, J. Zhang, Q. Ye, Programmed cell death-1 (PD-1) checkpoint blockade in combination with a mammalian target of rapamycin inhibitor restrains hepatocellular carcinoma growth induced by hepatoma cell-intrinsic PD-1. *Hepatology* **66**, 1920–1933 (2017).
28. K. Le Gal, C. Wiel, M. X. Ibrahim, M. Henricsson, V. I. Sayin, M. O. Bergo, Mitochondria-targeted antioxidants MitoQ and MitoTEMPO do not influence BRAF-driven malignant melanoma and KRAS-driven lung cancer progression in mice. *Antioxidants* **10**, 163 (2021).
29. E. Obrador, R. Salvador-Palmer, R. Lopez-Blanch, M. Oriol-Caballo, P. Moreno-Murciano, J. M. Estrela, N-acetylcysteine promotes metastatic spread of melanoma in mice. *Cancer* **14**, (2022).
30. E. Piskounova, M. Agathocleous, M. M. Murphy, Z. Hu, S. E. Huddlestun, Z. Zhao, A. M. Leitch, T. M. Johnson, R. J. DeBerardinis, S. J. Morrison, Oxidative stress inhibits distant metastasis by human melanoma cells. *Nature* **527**, 186–191 (2015).
31. P. E. Porporato, V. L. Payen, J. Perez-Escuredo, C. J. De Saedeleer, P. Danhier, T. Copetti, S. Dhup, M. Tardy, T. Vazeille, C. Bouzin, O. Feron, C. Michiels, B. Gallez, P. Sonveaux, A mitochondrial switch promotes tumor metastasis. *Cell Rep.* **8**, 754–766 (2014).
32. S. Kleffel, N. Lee, C. Lezcano, B. J. Wilson, K. Sobolewski, K. R. Saab, H. Mueller, Q. Zhan, C. Posch, C. P. Elco, A. DoRosario, S. S. Garcia, M. Thakuria, Y. E. Wang, L. C. Wang, G. F. Murphy, M. H. Frank, T. Schatton, ABCB5-targeted chemoresistance reversal inhibits Merkel cell carcinoma growth. *J. Invest. Dermatol.* **136**, 838–846 (2016).
33. M. Boyer, L. Cayrefourcq, F. Garima, V. Foulongne, O. Dereure, C. Alix-Panabieres, Circulating tumor cell detection and polyomavirus status in Merkel cell carcinoma. *Sci. Rep.* **10**, 1612 (2020).
34. M. Gao, M. Lin, R. A. Moffitt, M. A. Salazar, J. Park, J. Vacirca, C. Huang, K. R. Shroyer, M. Choi, G. V. Georgakis, A. R. Sasson, M. A. Talamini, J. Kim, Direct therapeutic targeting of immune checkpoint PD-1 in pancreatic cancer. *Br. J. Cancer* **120**, 88–96 (2019).

35. F. Liotti, N. Kumar, N. Prevete, M. Marotta, D. Sorriento, C. Ierano, A. Ronchi, F. Z. Marino, S. Moretti, R. Colella, E. Puxeddu, S. Paladino, Y. Kano, M. Ohh, S. Scala, R. M. Melillo, PD-1 blockade delays tumor growth by inhibiting an intrinsic SHP2/Ras/MAPK signalling in thyroid cancer cells. *J. Exp. Clin. Cancer Res.* **40**, 22 (2021).
36. K. G. de la Cruz Lopez, M. E. Toledo Guzman, E. O. Sanchez, A. G. Carrancá, mTORC1 as a regulator of mitochondrial functions and a therapeutic target in cancer. *Front. Oncol.* **9**, 1373 (2019).
37. D. Lv, L. Guo, T. Zhang, L. Huang, PRAS40 signaling in tumor. *Oncotarget* **8**, 69076–69085 (2017).
38. B. Perillo, M. Di Donato, A. Pezone, E. Di Zazzo, P. Giovannelli, G. Galasso, G. Castoria, A. Migliaccio, ROS in cancer therapy: The bright side of the moon. *Exp. Mol. Med.* **52**, 192–203 (2020).
39. C. Martins, M. Silva, E. Rasbach, P. Singh, Y. Itoh, J. B. Williams, E. Statham, A. Meurer, D. V. Martinez, A. Brandenburg, M. V. Heppt, S. R. Barthel, T. Schatton, Distinct antibody clones detect PD-1 checkpoint expression and block PD-L1 interactions on live murine melanoma cells. *Sci. Rep.* **12**, 12491 (2022).
40. T. Schatton, U. Schutte, N. Y. Frank, Q. Zhan, A. Hoerning, S. C. Robles, J. Zhou, F. S. Hodi, G. C. Spagnoli, G. F. Murphy, M. H. Frank, Modulation of T-cell activation by malignant melanoma initiating cells. *Cancer Res.* **70**, 697–708 (2010).
41. S. P. D'Angelo, C. Lebbe, L. Mortier, A. S. Brohl, N. Fazio, J. J. Grob, N. Prinzi, G. J. Hanna, J. C. Hassel, F. Kiecker, S. Georges, B. Ellers-Lenz, P. Shah, G. Guzel, P. Nghiem, First-line avelumab in a cohort of 116 patients with metastatic Merkel cell carcinoma (JAVELIN Merkel 200): Primary and biomarker analyses of a phase II study. *J. Immunother. Cancer* **9**, e002646 (2021).
42. N. A. Giraldo, P. Nguyen, E. L. Engle, G. J. Kaunitz, T. R. Cottrell, S. Berry, B. Green, A. Soni, J. D. Cuda, J. E. Stein, J. C. Sunshine, F. Succaria, H. Xu, A. Ogurtsova, L. Danilova, C. D. Church, N. J. Miller, S. Fling, L. Lundgren, N. Ramchurren, J. H. Yearley, E. J. Lipson, M. Cheever, R. A. Anders, P. T. Nghiem, S. L. Topalian, J. M. Taube, Multidimensional, quantitative assessment of PD-1/PD-L1 expression in patients with Merkel cell carcinoma and association with response to pembrolizumab. *J. Immunother. Cancer* **6**, 99 (2018).
43. E. J. Lipson, J. G. Vincent, M. Loyo, L. T. Kagohara, B. S. Luber, H. Wang, H. Xu, S. K. Nayar, T. S. Wang, D. Sidransky, R. A. Anders, S. L. Topalian, J. M. Taube, PD-L1 expression in the Merkel cell carcinoma microenvironment: Association with inflammation, Merkel cell polyomavirus and overall survival. *Cancer Immunol. Res.* **1**, 54–63 (2013).
44. H. Dong, S. E. Strome, D. R. Salomao, H. Tamura, F. Hirano, D. B. Flies, P. C. Roche, J. Lu, G. Zhu, K. Tamada, V. A. Lennon, E. Celis, L. Chen, Tumor-associated B7-H1 promotes T-cell apoptosis: A potential mechanism of immune evasion. *Nat. Med.* **8**, 793–800 (2002).
45. K. T. Flaherty, F. S. Hodi, D. E. Fisher, From genes to drugs: Targeted strategies for melanoma. *Nat. Rev. Cancer* **12**, 349–361 (2012).
46. J. C. Becker, A. Stang, J. A. DeCaprio, L. Cerroni, C. Lebbe, M. Veness, P. Nghiem, Merkel cell carcinoma. *Nat. Rev. Dis. Primers.* **3**, 17077 (2017).
47. V. Tkachev, S. Goodell, A. W. Opipari, L. Y. Hao, L. Franchi, G. D. Glick, J. L. Ferrara, C. A. Byersdorfer, Programmed death-1 controls T cell survival by regulating oxidative metabolism. *J. Immunol.* **194**, 5789–5800 (2015).
48. D. A. Hildeman, T. Mitchell, J. Kappler, P. Marrack, T cell apoptosis and reactive oxygen species. *J. Clin. Invest.* **111**, 575–581 (2003).
49. M. Dermit, P. Casado, V. Rajeeve, E. H. Wilkes, D. E. Foxler, H. Campbell, S. Critchlow, T. V. Sharp, J. G. Gribben, R. Unwin, P. R. Cutillas, Oxidative stress downstream of mTORC1 but not AKT causes a proliferative defect in cancer cells resistant to PI3K inhibition. *Oncogene* **36**, 2762–2774 (2017).
50. C. Glorieux, X. Xia, Y. Q. He, Y. Hu, K. Cremer, A. Robert, J. Liu, F. Wang, J. Ling, P. J. Chiao, P. Huang, Regulation of PD-L1 expression in K-ras-driven cancers through ROS-mediated FGFR1 signaling. *Redox Biol.* **38**, 101780 (2021).
51. C. Roux, S. M. Jafari, R. Shinde, G. Duncan, D. W. Cescon, J. Silvester, M. F. Chu, K. Hodgson, T. Berger, A. Wakeham, L. Palomero, M. Garcia-Valero, M. A. Pujana, T. W. Mak, T. L. McGaha, P. Cappello, C. Gorrini, Reactive oxygen species modulate macrophage immunosuppressive phenotype through the up-regulation of PD-L1. *Proc. Natl. Acad. Sci.* **116**, 4326–4335 (2019).
52. C. H. Chang, J. Qiu, D. O'Sullivan, M. D. Buck, T. Noguchi, J. D. Curtis, Q. Chen, M. Gindin, M. M. Gubin, G. J. van der Windt, E. Tonc, R. D. Schreiber, E. J. Pearce, E. L. Pearce, Metabolic competition in the tumor microenvironment is a driver of cancer progression. *Cell* **162**, 1229–1241 (2015).
53. N. Patsoukis, K. Bardhan, P. Chatterjee, D. Sari, B. Liu, L. N. Bell, E. D. Karoly, G. J. Freeman, V. Petkova, P. Seth, L. Li, V. A. Boussiotis, PD-1 alters T-cell metabolic reprogramming by inhibiting glycolysis and promoting lipolysis and fatty acid oxidation. *Nat. Commun.* **6**, 6692 (2015).
54. S. Ando, C. M. Perkins, Y. Sajiki, C. Chastain, R. M. Valanparambil, A. Wieland, W. H. Hudson, M. Hashimoto, S. S. Ramalingam, G. J. Freeman, R. Ahmed, K. Araki, mTOR regulates T cell exhaustion and PD-1-targeted immunotherapy response during chronic viral infection. *J. Clin. Invest.* **133**, e160025 (2023).
55. H. Chi, Regulation and function of mTOR signalling in T cell fate decisions. *Nat. Rev. Immunol.* **12**, 325–338 (2012).
56. J. Deng, A. D. Liu, G. Q. Hou, X. Zhang, K. Ren, X. Z. Chen, S. S. C. Li, Y. S. Wu, X. Cao, N-acetylcysteine decreases malignant characteristics of glioblastoma cells by inhibiting Notch2 signaling. *J. Exp. Clin. Cancer Res.* **38**, 2 (2019).
57. Y. S. Im, Y. K. Ryu, E. Y. Moon, Mouse melanoma cell migration is dependent on production of reactive oxygen species under normoxia condition. *Biomol. Ther.* **20**, 165–170 (2012).
58. M. J. Scheffel, G. Scurti, M. M. Wyatt, E. Garrett-Mayer, C. M. Paulos, M. I. Nishimura, C. Voelkel-Johnson, N-acetyl cysteine protects anti-melanoma cytotoxic T cells from exhaustion induced by rapid expansion via the downmodulation of Foxo1 in an Akt-dependent manner. *Cancer Immunol. Immunother.* **67**, 691–702 (2018).
59. K. Chamoto, P. S. Chowdhury, A. Kumar, K. Sonomura, F. Matsuda, S. Fagarasan, T. Honjo, Mitochondrial activation chemicals synergize with surface receptor PD-1 blockade for T cell-dependent antitumor activity. *Proc. Natl. Acad. Sci. U.S.A.* **114**, E761–E770 (2017).
60. M. A. Dickson, W. C. Hahn, Y. Ino, V. Ronfard, J. Y. Wu, R. A. Weinberg, D. N. Louis, F. P. Li, J. G. Rheinwald, Human keratinocytes that express hTERT and also bypass a p16^{INK4a}-enforced mechanism that limits life span become immortal yet retain normal growth and differentiation characteristics. *Mol. Cell. Biol.* **20**, 1436–1447 (2000).
61. T. Schatton, Y. Itoh, C. Martins, E. Rasbach, P. Singh, M. Silva, K. Mucciarone, M. V. Heppt, J. Geddes-Sweeney, K. Stewart, A. Brandenburg, J. Liang, C. J. Dimitroff, M. C. Mihm, J. Landsberg, C. Schlapbach, C. G. Lian, G. F. Murphy, T. S. Kupper, M. R. Ramsey, S. R. Barthel, Inhibition of melanoma cell-intrinsic Tim-3 stimulates MAPK-dependent tumorigenesis. *Cancer Res.* **82**, 3774–3784 (2022).
62. S. S. Pendse, S. Behjati, T. Schatton, A. Izawa, M. H. Sayegh, M. H. Frank, P-glycoprotein functions as a differentiation switch in antigen presenting cell maturation. *Am. J. Transplant.* **6**, 2884–2893 (2006).
63. T. Schatton, J. Yang, S. Kleffel, M. Uehara, S. R. Barthel, C. Schlapbach, Q. Zhan, S. Dudeney, H. Mueller, N. Lee, J. C. de Vries, B. Meier, S. Vander Beken, M. A. Kluth, C. Ganss, A. H. Sharpe, A. M. Waaga-Gasser, M. H. Sayegh, R. Abdi, K. Scharffetter-Kochanek, G. F. Murphy, T. S. Kupper, N. Y. Frank, M. H. Frank, ABCB5 identifies immunoregulatory dermal cells. *Cell Rep.* **12**, 1564–1574 (2015).
64. M. Hosseini, H. R. Rezvani, N. Aroua, C. Bosc, T. Farge, E. Saland, V. Guyonnet-Duperat, S. Zaghdoudi, L. Jarrou, C. Larrue, M. Sabatier, P. L. Mouchel, M. Gotanegre, M. Piechaczyk, G. Bossis, C. Recher, J. E. Sarry, Targeting myeloperoxidase disrupts mitochondrial redox balance and overcomes cytarabine resistance in human acute myeloid leukemia. *Cancer Res.* **79**, 5191–5203 (2019).
65. Z. Yang, Z. Lei, B. Li, Y. Zhou, G. M. Zhang, Z. H. Feng, B. Zhang, G. X. Shen, B. Huang, Rapamycin inhibits lung metastasis of B16 melanoma cells through down-regulating alphav integrin expression and up-regulating apoptosis signaling. *Cancer Sci.* **101**, 494–500 (2010).

Acknowledgments: We thank J. Schnabel for technical assistance. **Funding:** This work was supported by the following funding sources: Dermatology Foundation Research Grant (T.S.); American Skin Association Milstein Research Scholar Award (T.S.); Brigham Research Institute, Brigham and Women's Hospital Fund to Sustain Research Excellence (T.S.); National Institutes of Health, grants R01CA190838 (T.S.), R01CA247957 (S.R.B. and T.S.), and R01CA258637 (S.R.B. and T.S.); Harvard Stem Cell Institute Developmental Project Grant (M.R.R. and T.S.); German Research Foundation (DFG) Walter Benjamin Scholarship (E.R.); German Society of Dermatopathology (ADH) Martin Mihm Fellowship (M.V.H.); PhRMA Foundation Postdoctoral Fellowship (A.C.); Austrian Society of Dermatology and Venereology (ÖGDV) Klaus-Wolff Fellowship (J.H. and C.P.); Austria's Agency for Education and Internationalisation (OeAD) Marietta Blau-Grant (J.H.); Bayer Foundation Carl Duisberg Fellowship (A.B.); and Outrun the Sun Melanoma Research Scholar Award (C.P.). **Author contributions:** Conceptualization: C.M., C.P., S.R.B., and T.S. Methodology: C.M., E.R., M.V.H., P.S., Z.K., J.H., A.C., K.M., S.K., A.B., W.H., N.N.R., J.A.D., M.T., G.F.M., M.R.R., C.P., S.R.B., and T.S. Investigation: C.M., E.R., M.V.H., P.S., Z.K., J.H., A.C., K.M., S.K., A.B., N.N.R., J.A.D., M.T., M.R.R., and C.P. Visualization: C.M., E.R., M.V.H., P.S., Z.K., K.M., S.K., C.P., S.R.B., and T.S. Supervision: S.R.B. and T.S. Writing—original draft: C.M., S.R.B., and T.S. Writing—review and editing: C.M., E.R., M.V.H., P.S., Z.K., J.H., A.C., K.M., S.K., A.B., W.H., N.N.R., J.A.D., M.T., G.F.M., M.R.R., C.P., S.R.B., and T.S. **Competing interests:** J.A.D. has a sponsored research agreement with Kymera Therapeutics. M.T. has served as a consultant for Incyte. C.P. received honoraria and travel support from Almirall, AbbVie, BMS, Pelpharma, Novartis, LEO Pharma, Galderma, Roche, Celgene, Iovance, SUNpharma, Sanofi Genzyme, MSD, Pfizer, and Pierre-Fabre, all unrelated to this work. The authors declare that they have no other competing interests. **Data and materials availability:** All data needed to evaluate the conclusions in the paper are present in the paper and/or the Supplementary Materials. Additional data generated in this study are publicly available in GenBank, under accession numbers OQ594425 to OQ594428, or the Harvard Dataverse at https://doi.org/10.7910/DVN/XXJTKY. All materials generated in this study are available from the corresponding author, T.S.

Submitted 25 April 2023
Accepted 20 December 2023
Published 19 January 2024
10.1126/sciadv.adi2012

ScienceAdvances

Tumor cell–intrinsic PD-1 promotes Merkel cell carcinoma growth by activating downstream mTOR-mitochondrial ROS signaling

Christina Martins, Erik Rasbach, Markus V. Heppt, Praveen Singh, Zsofi Kulcsar, Julia Holzgruber, Asmi Chakraborty, Kyla Mucciarone, Sonja Kleffel, Anne Brandenburg, Wolfram Hoetzenecker, Nuh N. Rahbari, James A. DeCaprio, Manisha Thakuria, George F. Murphy, Matthew R. Ramsey, Christian Posch, Steven R. Barthel, and Tobias Schatton

Sci. Adv. **10** (3), eadi2012. DOI: 10.1126/sciadv.adi2012

Science Advances (ISSN 2375-2548) is published by the American Association for the Advancement of Science. 1200 New York Avenue NW, Washington, DC 20005. The title *Science Advances* is a registered trademark of AAAS.